STUDY OF THE RISK OF FROSTBITE IN HUMANS WITH THE HELP OF A TRANSIENT 3D FINGER MODEL

by

PRUDHVI KRISHNA VENKATESH MANDA

B.Tech, Jawaharlal Nehru Technological University, 2007

A THESIS

submitted in partial fulfillment of the requirements for the degree

MASTER OF SCIENCE

Department of Mechanical and Nuclear Engineering
College of Engineering

KANSAS STATE UNIVERSITY
Manhattan, Kansas

2013

Approved by:

Major Professor
Steve Eckels

Copyright

Abstract

A new three dimensional transient human finger model was developed to predict the risk of frostbite in humans at different environmental conditions. The shape of the finger model was similar to that of a real human finger. Finite Element Techniques were used to build the finger model. Smith's Model (1991) energy balance equations were used to calculate the temperatures in the current finger model. The current 3D finger model was validated against the experimental data of Wilson (1976) and Santee (1990). The model agreed well with the Wilson experiments and with the cold test in Santee experiments. The comparison indicates that the current finger model can be used to adequately predict the human finger responses in different environments.

The current finger model was then tested in temperatures of 0, -10, -20, -25 and -30 ^{o}C and with different airspeeds 0, 3 and 6.8 m/s to assess the risk of frostbite in humans. Three resistances 0, 0.4 and 0.8 clo were used on the finger model to obtain responses in different environmental conditions. From the experimental results, an expression for safe glove resistance required to prevent frostbite in known temperatures was calculated. Also, the temperatures up to which a glove with known thermal resistance value can protect a human finger from frostbite was also computed.

Table of Contents

List of Figures

List of Tables

Nomenclature

Symbol	Symbol Definition and Units
Ast	Surface Area, cm^2
C_p	Specific heat, J/g- ^oC
D_{AB}	constant mass diffusivity
h	Heat transfer coefficient along surfaces, J/hr-cm^2- ^oC
h_{fg}	Latent Heat of vaporization, J/g
Ƙ	Heat conductivity, J/hr-cm- ^oC
M	Metabolic rate in the finger, J/hr
m_m''	Moisture evaporation rate from the skin surface ,g/hr-cm^2
m_{rsw}	Sweat rate per unit surface area, g/hr-cm^2
m_{sw}	Sweat Rate of the entire finger, J/hr
m_{skin}	Moisture accumulation on unit skin surface area, g/cm^2
P	Pressure or vapor pressure, kPa or mm Hg
Pr	Prandtl Number, dimensionless
q	Heat Transfer rate, J/hr-cm
q'''	Internal heat generation , J/hr-cm^3
r,θ,Z	Cylindrical coordinates
r,θ,ϕ	Spherical coordinates
r_o	Blood vessel radius, cm
r	Radius or radial distance from the center of the cylinder,cm
Re	Reynolds Number, dimensionless

RH	Relative Humidity, dimensionless
RQ	Respiratory quotient, ratio of the volumetric flow rate of exhaled carbon dioxide to that of inhaled oxygen
T	Temperature, ^{o}C
T_{sweat}	Sweating threshold, ^{o}C
t	Time, hr
V	Volume, cm^3
v	blood or air velocity in the axial direction, cm/hr
W	Humidity ratio, g H_2O/g dry air
w_b	Volumetric blood flow rate in the capillary bed, 1/hr
z	dimension along the axis of the respiratory tract or blood vessel, cm
ρ	Density , g/cm^3
μ	Viscosity, g/hr-cm

Subscript	**Symbol Definition and Units**
a	Artery
air	Environmental air
b	Blood
bv,basal	Basal Value
c	Convection
core	Core
con	Vasoconstriction
dil	Vasodilation

max	Maximum
min	Minimum
r	Radiation
res	Respiratory air
skin	Skin
sw, sweat	Sweat
sur	Surrounding
v	Vein

Superscript	**Symbol Definition and Units**
*	Saturation

Chapter 1 - Introduction

Frostbite is a common cold injury among humans exposed to cold temperatures. The risk of frost bite starts when outside temperatures fall below skin freezing point and increase significantly as winds increase, raising the rate of heat loss. The body parts away from the heart like fingers, ears, toes, cheeks and nose are most commonly affected by frostbite when continually exposed to cold conditions. The skin surface of the affected body part freezes during the initial stages of frost bite and the body part might become numb. If the body part is exposed for longer periods at cold conditions, the deep tissue of the affected body part freezes and without immediate medical attention, the body part may die and be lost. As frostbite has severe consequences, various experiments have been conducted on human beings to predict the skin freezing point temperatures.

The objective of this thesis is to develop a three dimensional finite element finger thermal model to predict the risk of frostbite in humans when exposed to cold conditions. Shitzer (1991 and 1997) developed one dimensional and two dimensional finger models to predict human finger responses at different temperatures. One of the limitations of the Shitzer model is that the heat transfer in the angular direction in the model was ignored. In reality, as the blood vessels run on either side of the bone in the human finger, heat transfer needs to be considered in all the directions in a finger model i.e. angular, axial and radial to achieve appropriate responses of the human finger. The other limitation is that the models developed by Shitzer were cylindrical in nature with no accurate representation of fingertip which is more highly susceptible to frostbite than the rest of the finger owing to its high surface area to volume ratio.

The three dimensional finger model developed in this thesis consists of a fingertip which is hemispherical in shape in addition to the cylindrical finger. The model is fully 3-D thus heat transfer occurs in angular, radial as well as in axial directions. The three dimensional finger model is made up of several triangular, rectangular and spherical elements. The blood vessels are represented by one dimensional element. Finite element techniques coupled with the energy, momentum and conservation of mass equations are the foundation of the current model. More detailed description is given in later chapters.

1.1 Background

The thermal response of the body is often studied by Thermal Physiologist. Background information on frostbite and the response of extremities from a Physiology perspective is reviewed in this section. Specifically, in this section, basic knowledge related to the finger anatomy, the arterio-venous anastomoses (AVA) in the finger, cold-induced vasodilatation (CIVD) which is a protective mechanism in the finger and frost bite- a common cold injury in the finger is discussed. It should be noted that one goal of the initial work of this thesis is to translate these physiology process to knowledge of fundamental heat transfer and control descriptions so they can be solved mathematically.

Fingers are the upper extremities (part of the hands) of the human body which are used to carry, move objects and are also used for sensation. A normal human being has five fingers- thumb, index finger, middle finger, ring finger and little finger. All the fingers are made up of three bones - distal phalanx, middle phalanx and proximal phalanx except for the thumb which does not contain a middle phalanx. The fingers are devoid of any muscles and fingers move with the help of muscles present in the palm and forearm. Radial and ulnar arteries

distribute blood into the fingers and radial and ulnar veins move blood out of the fingers. Raynaud's phenomenon and frostbite are cold injuries in the finger caused by extreme cold temperatures. Raynaud's phenomenon is a disorder which causes the discoloration of body extremities and occurs when the blood vessels in the extremities overreact at cold temperatures or stress, thereby reducing the blood supply in the extremities. In general, young women are more susceptible to Raynaud's phenomena. Frost bite has been explained in detail at the end of this section.

Arterio-venous anastomoses (AVA) are thermoregulatory organs in fingers and toes that regulate the blood flow and heat transfer to the surroundings in all conditions (Vanggaard, Kuklane, Holmer, & Smolander, 2012). AVAs are thick walled vessels present between the arterioles and venules located deeper in the skin of the extremities. However, AVAs are not fixed structures, they develop when the blood requirement in the fingertip increases and disappear when no longer needed. AVAs are also present in the hands, feet, ears and nose of a human and are thought to play a major role in cold-induced vasodilatation (CIVD) mechanism (Daanen, Koedam, & Cheung, 2012).

CIVD is a protective mechanism in the extremities of the human body that protects them from cold injuries. When a human is exposed to cold conditions without wearing sufficient clothing, the finger skin temperature of the human decreases. When the finger skin temperature falls below 15 ^{o}C, a sudden periodic vasodilatation is observed in the finger of some individuals. This opening of the blood vessels leads to increased blood flow and indirectly increases local skin temperature ((Daanen, Koedam, & Cheung, 2012). CIVD is believed to occur due to the sudden decrease in the release of neurotransmitters from the sympathetic nerves to the thick wall of the AVA due to local cold temperature. CIVD

response varies in different individuals depending on their age, gender, diet, acclimatization and adaptation in cold environments. Individuals with reduced CIVD response are more susceptible to frostbite (Daanen H. A., 2003).

Frostbite is a localized, cold injury to the body caused due to skin and other tissues freezing at low temperatures. Frostbite generally occurs when the body is exposed to temperatures below the skin freezing point for extended periods of time. Whenever the body is exposed to lower temperatures for long periods, the body's primary aim is to stay alive first and stay functioning second. In prolonged cold exposure, the blood flow to extremities is reduced so as to send more blood to the vital organs in the body. With reduced blood flow in the extremities, their skin temperature decreases. As the skin temperature in the extremities deceases beyond a certain point, the skin tissue freezes. This results in the formation of ice crystals in the tissue. When this happens, frostbite is said to have initiated. In the early stages of frostbite, the affected skin area develops white patches and the skin is frozen. This stage is often called frostnip. The person might experience burning, itching or numbness in the affected area. If the affected area is still exposed to extreme conditions, deep frostbite occurs. The muscles, blood vessels and all other tissues in the affected area freeze and the skin becomes hard. The affected area might lose its dexterity temporarily and sometimes even permanently. The skin area develops purplish blisters which turn black and are generally blood filled. In most cases, the affected fingers or toes might have to be amputated.

1.2 Thesis Outline

In Chapter 1, the objective of this thesis has been presented and a brief background of human finger anatomy, blood vessels in the finger, CIVD and frostbite has been presented. In the current three dimensional finger model, CIVD was not included as the occurrence of

CIVD in humans is random where in few cases, it might not even occur. Arterio-venous anastomoses were also not included in the present model as there is very limited accurate information about the AVAs at present. In Chapter 2, literature reviews on previous human and finger models will be presented. In addition to the body models, literature reviews on experiments conducted to determine finger blood flow and finger freezing point will also presented. The finger thermal model will be developed in Chapter 3 and, in Chapter 4 the solution method for the finger model will be presented. The finger model will be validated against experimental data in Chapter 5. The experiments performed on the finger model and the experimental results obtained will be analyzed and discussed in Chapter 6. In Chapter 7, a conclusion and further recommendations on the current model will be presented.

Chapter 2 - Literature Review

Human Thermal Models developed by Stolwijk (1970), Wissler (1985), Smith (1991) and Salloum (2007) are reviewed in this chapter. Stolwijk, Wissler and Smith human models differ in the number of body segments used, the circulatory system model, human responses incorporated and the intended applications of the model. For example, Salloum's model provides a better arterial representation of the human circulatory system than the other models.

The next section reviews the available literature on human figure response to cold temperature conditions. Studies done by Keatinge and Cannon (1960), Wilson et al. (1976) and Santee (1990) provide valuable information about cold injury to fingers and document that fingers are more susceptible to extreme temperatures. This chapter reviews the work of Burton (1939), Greenfield et al. (1951), Zweifler et al. (1967), Coffman (1972) and Cooke et al. (1990) who all provided blood flow information. Models developed specifically for the finger are reviewed in the final section of the chapter.

2.1 Human Thermal Models

Human thermal modeling as a science was based on analog simulations in the early days. For example, Wyndham and Atkins (1969) developed an analog simulation for studying human responses. With the onset of digital computers, more complex models were developed. The most commonly used models are Gagge (1971), Stolwijk (1970) and Wissler (1985) model. Gagge used a two node model to represent the human body; Stolwijk used Gagge's idea and divided the human body into five segments. Wissler provided a more complex representation by dividing the human body into fifteen segments. Several human thermal models were developed since Wissler published his model but most are a modification or an extension of the based models mentioned above. For example, Smith's model (1991) is roughly based on Stolwijk and Wissler's model;

she divided the human body into fifteen cylindrical elements. The following subsections review the most important models.

2.1.1 Stolwijk Model

Stolwijk (1970) developed a human thermal model based on Gagge's idea. Stolwijk divided the body into six segments. The trunk, arms, legs, hands and feet are represented by cylindrical elements and the head by spherical element. Each body segment is divided into four concentric shells – core, muscle, fat and skin. The head core and the trunk core are assumed to be the brain tissue and internal organs, while the core layers of arms, legs, hand and feet are assumed bone.

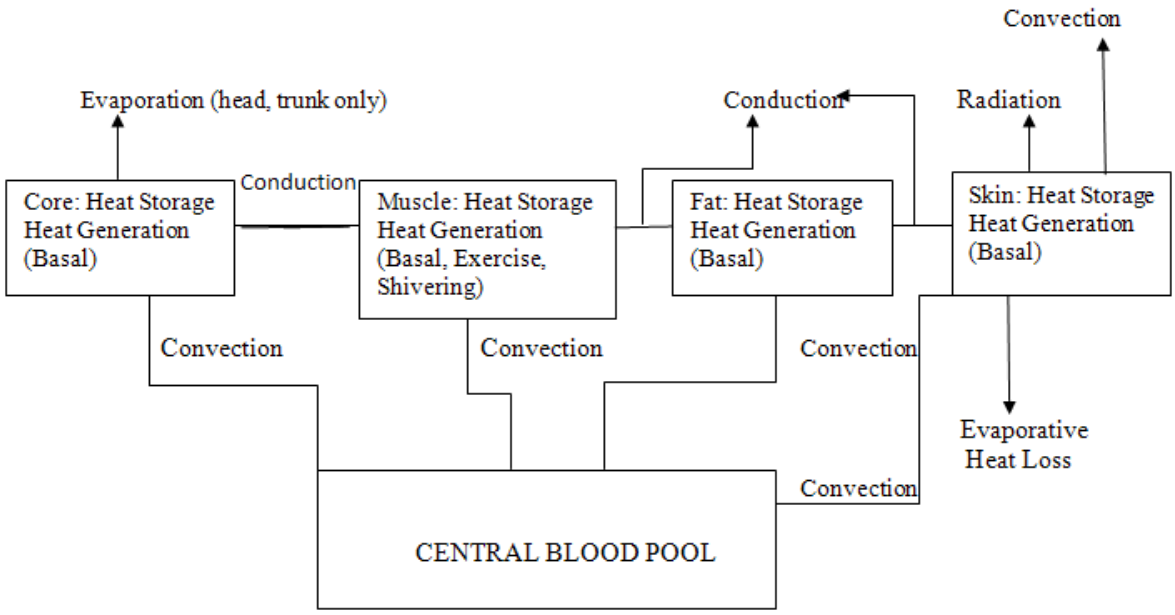

Figure 2.1 Schematic of Stolwijk's model (Block Diagram for One Segment)

A hypothetical central blood compartment links the six segments via appropriate blood flows for each segment of the body. Heat balance equations are written for each body layer and the blood pool resulting in 25 heat balance equations that form the core of the model. Heat transfer through the core, muscle and fat body layers occurs due to conduction and convection.

The skin layer exchanges energy with the environment through evaporation, conduction and convection.

Control equations are written for the blood flow rate in the skin, rate of heat production due to shivering and sweat rate from the skin surface. These control equations are assumed to be functions of tissue temperature signals, defined as the deviations of the tissue temperature from the temperatures at thermo neutrality and the rate of change of tissue temperatures. A warm head core and warm skin temperature signal governs vasodilation and rate of evaporative heat loss at the skin surface whereas cold signals from both these regions govern the shivering metabolic heat generation rate. The cold skin temperature signal governs vasoconstriction.

Stolwijk connected the individual body elements through blood flow, hence providing an improved representation of the circulatory system. Blood flow to the elements also allowed him to incorporate the effect of heat convection between tissue and vessel. Stolwijk's Model can only resolve radial temperature distribution in each individual body part limiting application in nonuniform environmental conditions. Stolwijk's Model also does not consider sweat accumulation on the skin surface.

2.1.2 Wissler Model

Wissler (1964, 1966 and 1985) developed one of the most complete human thermal models. In the model, the body is divided into fifteen elements – head, thorax, abdomen, upper arms, lower arms, thighs, calves, hands and feet. Each element consists of a three part vascular system made up of arteries, veins and capillaries. All the fifteen elements connect through the vascular system. An arterial and venous blood pool in each element models the large arteries and veins in the human body. In Wissler's model, the blood flow starts with the arterial blood entering each element which then flows into the capillaries of that element or into the arteries of

the more distal elements. The blood leaving the capillaries then flows into the veins where it mixes with the venous return of the more distal elements. This mixed venous stream then returns to the heart and lungs before entering the arterial system for redistribution.

The main sources of heat in the model are the metabolic reactions. Energy balance equations are written for each element, which includes the rate of thermal energy accumulated, conductive heat transfer in radial direction, metabolic heat generation, and convective heat transfer due to blood flow in the capillaries, venous and arterial blood pools, as in Equation 2-1. The heat conduction in the longitudinal direction of the element is neglected.

$$\rho_i c_i \frac{\partial T_i}{\partial t} = \frac{1}{r}\frac{\partial}{\partial r}(k_i r \frac{\partial T_i}{\partial r}) + q_{mi} + \rho_b c_b w_b (T_{ai} - T_i) + h_{ai}(T_{ai} - T_i) + h_{vi}(T_{vi} - T_i) \qquad (2\text{-}1)$$

where ρ_i is the density of tissue, c_i is the specific heat of tissue, T is the instantaneous temperature of tissue, k_i is the conductivity of tissue, q_{mi} is the metabolic generation of tissue, ρ_b is the density of blood, c_b is the specific heat of blood, w_b is the volumetric rate of blood, T_{ai} is the arterial temperature of tissue, T_{vi} is the venous temperature of tissue, h_{ai} is the convective heat transfer coefficient between arteries and tissue, h_{vi} is the convective heat transfer coefficient between venous and tissue.

Two additional energy balance Equations (2-2) and (2-3) which are partial differential equations for each blood pool i.e.; arterial and venous blood pool are written for each element.

$$m_{ai} c_b \frac{dT_{ai}}{dt} = \rho_b c_b w_{ai}(T_{am} - T_{ai}) + 2\pi l_i \int_0^{a_i} h_{ai}(T_i - T_{ai}) r dr + h_{avi}(T_{vi} - T_{ai}) \qquad (2\text{-}2)$$

$$m_{vi} c_b \frac{dT_{vi}}{dt} = \rho_b c_b w_{vi}(T_{vn} - T_{vi}) + 2\pi l_i \int_0^{a_i} (\rho_b c_b w_{vi} + h_{ai})(T_i - T_{vi}) r dr + h_{avi}(T_{ai} - T_{vi}) \qquad (2\text{-}3)$$

Equation (2-2) states that the rate of heat storage in the arterial pool is equal to the rate at which heat flows into the arterial pool from the adjacent element, from the tissue and from the venous pool. Equation (2-3) represents the same for the venous pool.

A series of boundary and initial conditions which include the heat exchange processes with the environment like convection, radiation and evaporation of moisture are specified at the surface of the skin. Wissler solved the differential equations using Crank- Nicholson's implicit finite difference method.

Wissler tested his model in varying environmental conditions and activity levels. The results from the model closely approximated the experimental data. However, because Wissler considered only radial heat conduction in his model, as Stolwijk model, his model is limited to applications involving uniform environmental conditions surrounding each body part. But, unlike Stolwijk model, each element in the Wissler's model communicates with the adjacent element through blood flow which is more true to life than any other model.

2.1.3 Smith Model

Smith's (1991) human thermal model was based on Stolwijk and Wissler's model. Smith's model is transient and three dimensional developed using finite element method so it can be used in different environmental conditions. Smith divided the human thermal system into two interactive systems – controlled system which includes body tissues, circulatory, respiratory systems and control system which initiates and controls the physiological responses in the model.

Smith divided the body into 15 cylindrical parts as shown in Figure 2.2: head, neck, torso, upper arms, forearms, hands, thighs, calves and feet. Each of these cylinders is divided radially into concentric shells, axially and angularly into tissue elements (shown in Figure 2.3). Smith's model consists of two types of tissue elements: One is the triangular 3D element and the

other is the trapezoidal 3D element (shown in Figure 2.4). The triangular 3D element is located in the innermost concentric shell and the trapezoidal 3D element is located in all other concentric shell. In Smith's model, each tissue element is assigned to one of the following types: brain, abdomen, fat, lung, bone, muscle and skin.

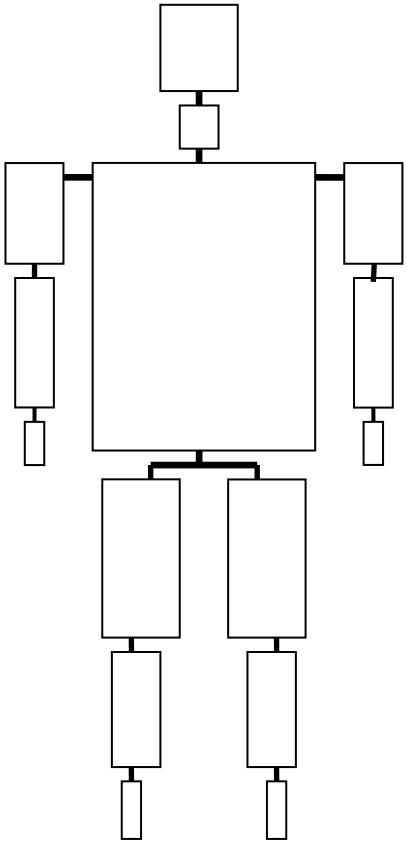

Figure 2.2 Schematic of Smith's Model

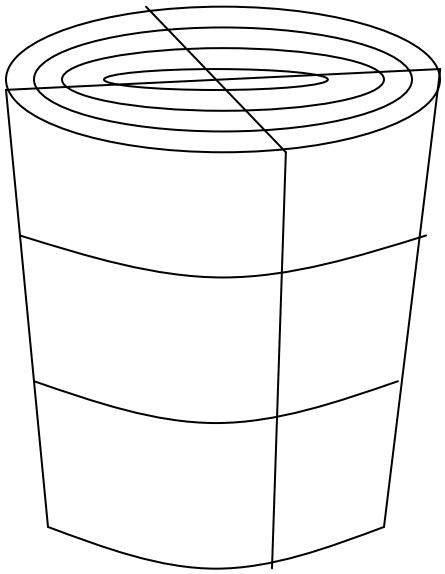

Figure 2.3 Layout of upper arm in Smith's Model

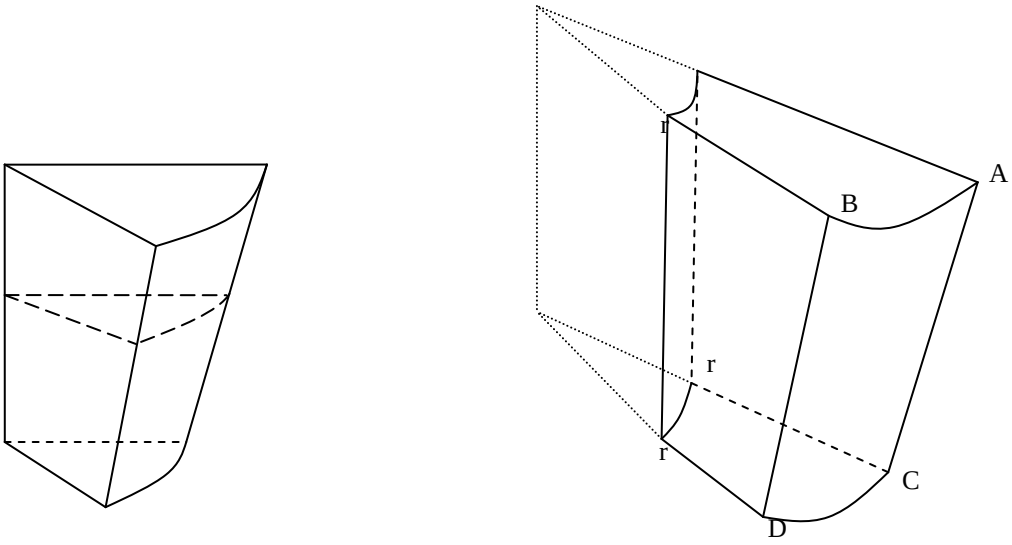

Figure 2.4 3D Triangular and Trapezoidal element

Smith represented the circulatory system as an intricate network of blood vessels which transports blood to the body tissues. The blood flow originates and terminates at the heart, which is represented by two points, one for the right atrium and one for the left ventricle. All the blood vessels are 1D element and are located between the 3D elements. The blood flow is considered one dimensional, incompressible, laminar, steady, fully developed flow and the blood flow rate is defined as a function of the metabolic rate and the thermal state of the body.

The respiratory system is simulated as a dual tract respiratory model. As in the circulatory system, the respiratory system is modeled as 1D. During respiration, heat and mass transfer takes place between the air and the surrounding tissue.

Three factors determine the heat and mass transfer in Smiths model: ambient conditions, body temperature distribution and humidity ratio inside the respiratory tract. The model uses the following energy balance equations:

For a blood vessel:

$$\rho C_p \frac{\partial T}{\partial t} = \kappa . \nabla . \nabla T - \rho C_p v' \frac{dT}{dz} \qquad (2\text{-}4)$$

For a Tissue element:

$$\rho C_p \frac{\partial T}{\partial t} = \kappa . \nabla . \nabla T + q''' \qquad (2\text{-}5)$$

As there is mass and heat transfer during respiration, a mass balance equation is written for a given respiratory tract element:

$$D_{AB} \frac{d^2 W_{air}}{dz^2} - v_{res} \frac{dW_{air}}{dz} = 0 \qquad (2\text{-}6)$$

The air velocity in the respiratory tract was calculated from the volumetric oxygen consumption rate which in turn is a function of the metabolic rate.

Volumetric oxygen consumption rate:

$$V_{O2} = \frac{M}{\left[21.12\left(0.23RQ + 0.77\right)\right]} \qquad (2\text{-}7)$$

Velocity of air in respiratory tract:

$$V_{res} = \frac{V_{O2}}{\pi r_o^{\,2}} \qquad (2\text{-}8)$$

The transient temperature and pressure distributions for the blood were determined by the following momentum and energy equations.

$$\rho_b C_{p,b} \frac{\partial T_b}{\partial t} = K_b \left(d^2 T_b / dz\right) - \rho_b C_{p,b} B_{bl} \frac{dT_b}{dz} \qquad (2\text{-}9)$$

$$v_{bl} = - \frac{\pi r_o^{\,2}}{8\mu} \left(\frac{dP_b}{dz} \right) \qquad (2\text{-}10)$$

Smith considered the core and skin temperatures as a major influence on the thermal responses of the human body. Smith used available experimental data to design control equations for skin blood vessel radii, sweat rate and shivering metabolic rate as functions of core and skin temperatures. The derivation of control system equations for vasomotor response in the human body was based on the assumption of thermoneutrality. The development of the control equation for the sweat rate and the increased metabolic rate caused by shivering were based on the findings published by Benzinger (1970).

Smith simulated warm, cold and neutral environments with various levels of activity and compared the model responses with available experimental data. It was found that the Smith's model predictions displayed the same curve patterns as those of the experimental data with no significant differences. Smith expanded on the Wissler and Stolwijk model by dropping most of the empirical correlations except for the description of the blood flow. Smith also refined the vascular system model by making it more realistic.

2.1.4 Salloum Model

Salloum (2007) presented a multi-segmented model based on Stolwijk work. The focus was to develop a realistic representation of the arterial system including the blood flow pulsation.

The human body is divided into fifteen cylindrical segments. The head and neck is combined into one segment whereas the trunk is divided into two segments. Each segment is further subdivided into four layers- core, skin, artery blood, vein blood and each layer is assumed to have a uniform temperature.

The human circulatory system is made up of 128 vessels. In any body segment, the blood leaving the arteries and entering the capillaries is divided into blood flowing in the core and blood flowing into the skin layer. Therefore, the blood flow entering each segment will divide into skin blood flow in the considered segment and blood flow entering the adjacent segment. The opposite takes place in the veins for the same segment. The flow in veins is assumed non–pulsatile and is equal to the mean value of the corresponding artery flow. Vein diameter is assumed twice the artery diameter.

The thermal responses in the model are predicted with the help of energy balance equations written for segment layer as shown in the following equations.

Core:

$$C_{cr}.\ \frac{dT_{cr}}{dt} = M_{cr} + M_{shiv} - W - \alpha.Q_{res} - Q_{cr\text{-}sk} - \sum_{arteries} h_{artery} A_{artery} (T_{cr} - T_{bl,a}) \qquad (2\text{-}11)$$

$$- \sum_{veins} h_{vein} A_{vein} (T_{cr} - T_{bl,v}) + (m_{perf,cr} + m_{perf,sk}) c_{bl} (T_{bl,a} - T_{cr})$$

In Equation (2-11), the left hand side represents the rate of change of stored energy in the core. The terms on the right hand side represents the basal and segmental shivering metabolic rate, heat dissipated by respiration, heat exchange between the core and skin, heat transfer with the surrounding blood vessels, blood perfusion.

Skin:

$$C_{sk}\frac{dT_{sk}}{dt} = M_{sk}+Q_{cr\text{-}sk} - A_{sk}[h_c(T_{sk}\text{-}T_{\infty}) + h_r(T_{sk}\text{-}T_{mrt}) + h_e(P_{sk}\text{-}P_{\infty})]$$

$$+m_{skin}.c_{bl}.(T_{cr} - T_{sk}) \qquad (2\text{-}12)$$

In the above equation, M_{sk} is the metabolic rate in the skin; A_{sk} is the exposed skin surface area. The terms on the right hand side represents metabolism, heat exchange between the core and skin, heat lost to the surroundings through convection, radiation, evaporation and heat transfer through the skin blood flow.

Artery:

$$\mathrm{C_{bl,a}}\frac{dT_{bl,a}}{dt} = \sum_{arteries} h_{artery}A_{artery}(T_{cr} - T_{bl,a}) + m_a c_{bl}(T_{bl,a,adjacent} - T_{bl,a}) \qquad (2\text{-}13)$$

Vein:

$$\mathrm{C_{bl,v}}\frac{dT_{bl,a}}{dt} = -\sum_{veins} h_{vein}A_{vein}(T_{cr} - T_{bl,\mathrm{v}}) + m_v c_{bl}(T_{bl,v,adjacent} - T_{bl,v})$$

$$+m_{perfusion,total}\, c_{bl}(T_{cr} - T_{bl,v}) \qquad (2\text{-}14)$$

In Equations (2-13) and (2-14), the left hand side represents the rate of energy stored in the blood vessels and the right hand side represents the heat transfer with the tissue and heat transfer due to perfusion. The arterial circulation system is validated against the published data of Mills et.al (1970) and simulation model of Avolio (1980). The skin temperature values of Salloum model showed an accuracy of $\pm 0.48^{o}$C to those of experimental data.

2.2 Temperature Experiments on Human Fingers

Human responses to different environmental conditions have been studied extensively for the past 100 years. In the current study, the focus is the response of the finger and specifically the dangers of frostbite. The freezing point of finger has been investigated by Siple and Passel in 1945. They used a cylinder filled three fourths with water and predicted the freezing of skin from a given temperature and air speed from a wind chill formula derived from the cooling rate of water in the cylinder. The wind chill formula was shown to be inaccurate due to questionable simplifications used to derive it. Keatinge and Cannon (1960), Wilson et al. (1970, 1976) conducted experiments on human subjects which provided better results than those of Siple and Passel. Keatinge and Cannon (1960) reported the true freezing point of fingers from experiments conducted in a brine solution at -1.9^{o}C. Wilson et al. used wind in his cold experiments to replicate a real environment and determined the freezing point of fingers. Santee (1990) determined the human finger responses at different temperatures and different metabolic rates of the body. During the experiments conducted by Santee, the human subjects were wearing dry or wet gloves on their hands.

2.2.1 Freezing-Point of Human Skin

Keatinge and Cannon (1960) conducted experiments on human fingers to determine the true freezing point of human skin. They used little fingers of healthy men and women aged 18-38 years. A rubber tourniquet at the base of the finger occluded blood flow in order to avoid fluctuations in temperature readings brought about by the blood flow. Skin temperature of the human fingers is measured with the help of thermocouples applied to the surface of the finger by zinc oxide plaster or is inserted for a length of 1cm into an intracutaneous track made in the deeper layers of the epidermis of the fingertip. The entire finger was dipped along with the

thermojunction and tourniquet in a mixture of ice and water to precool the set up to 0^{o}C. To determine the freezing point of human skin, the distal phalanx of the finger was dipped in a freezing mixture of ice and brine maintained at a temperature of -1.9±0.02^{o}C.In order to obtain the true freezing point of skin, Keatinge and Cannon inserted the thermocouple into an intracutaneous track covered with varying thicknesses of plaster. They found the true freezing point of human fingers to be between -0.53 and -0.65 ^{o}C.

Keatinge and Cannon also conducted experiments with blood circulations present in the human finger and without any precooling. The immersed fingers were reported to have frozen after four minutes. Keatinge and Cannon assumed that the cold vasodilatation (CIVD) which generally protects the extremities from freezing would take several minutes to start before which the fingers froze in the experiments conducted.

2.2.2 Freezing temperature of finger skin

Wilson, Goldman and Molnar (1976) induced frost nips in forty five male volunteers by exposing the fingers at -15^{o}C with various wind speeds. All the subjects lightly clothed, were precooled in a 25.5^{o}C room for 1 hour with 20% relative humidity. The same set of conditions was used during the frost bite test for the finger. For the frost bite experiment, the finger was inserted perpendicularly through two holes of a Plexiglas tube with the fingertip protruding out of the tube. Cold air was drawn from a large climatic chamber onto the lateral surface of the middle phalanx of the middle finger. The finger surface temperature was measured with the help of a thermocouple wire wrapped around the exposed finger.

Experiments were conducted at different temperatures and different windspeeds. Air temperature of -15 ± 1.0^{o}C was used along with the windspeeds of 6.8, 9 and 10 m/s. One test

was done with a combination of -12±1.0^{o}C and a windspeed of 10 m/s. The experiments lasted for 15 minutes unless frostnip occurred.

Wilson, Goldman and Molnar reported that the overall mean supercooled skin temperature at which frostnip appeared at -15^{o}C to be -9.4 ± 2.2 ^{o}C with the range being -3.4 to -13.8 ^{o}C. Wilson et.al observed that half of the frost nips occurred between -6 and -10^{o}C. They also reported the mean time to freeze (mean±SD) to be 8.4 ± 2.8 min at 6.8 m/s, 7.1 ±32 min at 9m/s, and 6.6 ± 3.1 min at 10 m/s. At -12 ^{o}C and 10 m/s, the mean time to freeze was 7.4 ± 3.1 min.

Wilson et.al also estimated the apparent freezing point of skin (T_e) with no supercooling with the help of regression formulae. They estimated T_e to be -2.4 ± 0.5 ^{o}C at 6.8m/s, -3.1 ± 0.5 ^{o}C at 9 m/s and -3.3 ± 0.4 ^{o}C at 10m/s. Wilson, Goldman and Molnar compared this result against the freezing point obtained by the tests conducted by Keatinge and Cannon. They observed that the calculated apparent freezing point at -15^{o}C was 1.2^{o}C lower to the true freezing point of skin determined by Keatinge and Cannon. Wilson et.al suggested that the freezing point of skin in cooling conditions with wind present to be lower.

2.2.3 Comparison of Light Duty Gloves under Wet and Dry Conditions

Santee, Endrusick and Pensotti (1990) measured finger temperatures of five volunteers wearing standard cold weather military uniform during three different experiments. During the experiments, the volunteers wore three different light duty gloves whose thermal insulation values varied from 0.124 to 0.118 $m^2C^o W^{-1}$. In one experiment, the volunteers walked on a treadmill for 120 minutes, in another experiment, the volunteers sat for 125 minutes and in the third experiment, the volunteers participated in contact simulation for 60 minutes. All the three experiments were conducted in a chamber with an air temperature of -6.7^{o}C (20^{o}F) and a wind

speed of 1.1 m/s (2.5mph).The sitting tests were repeated in a second chamber at 0^{o}C and the contact tests were repeated with wet gloves.

Rectal and finger temperatures, heart rate, and endurance times were measured for all the tests. The tests were continued for the entire simulation time unless the heart rate of a volunteer was 180bpm for 5 minutes, rectal temperature dropped to 35.5^{o}C and skin surface temperature dropped to 5^{o}C.

For the sitting tests, at -6.7^{o}C the left fingertip temperature dropped to 9^{o}C after 85 minutes while at 0^{o}C the fingertip temperature dropped to the same temperature after 105 minutes.

2.3 Blood Flow Experiments on Human Fingers

Blood flow in the human finger plays a decisive role in regulating the heat loss and temperature of the human being. The peripheral blood flow in the human changes with different environmental temperatures and is affected when the body needs to survive at extreme conditions. The finger blood flow is generally measured with a finger plethysmograph technique. Most of the finger blood flow experiments use this technique to determine the finger blood flow at different experimental conditions. However, Greenfield (1951) used a different technique where he constricted blood flow to the fingers in one hand and measured the blood flow rate difference in both the hands. Coffman (1972) used the finger plethysmograph technique to determine the total and nutritional blood flow in fingers. Cooke et al. (1990) determined that gender differences in the peripheral blood flow have an impact on increasing cases of Raynaud's disease in women. Blood flow tests conducted by Burton (1939), Greenfield (1951), Zweifler et al. (1967), Coffman (1972) and Cooke (1990) are discussed in this section.

2.3.1 Burton's Finger Blood Flow Test

Burton (1939) analyzed the effect of range and variability of blood flow in peripheral vessels in the control of body temperature. Burton chose fingers for his study as fingers contain arterial-venous anastomoses, which largely affects the amount and distribution of blood flow. Burton determined the blood flow through the fingers with the help of venous occlusion technique.

Burton conducted experiments on seven normal subjects and induced blood flow at extreme temperatures. Burton also used constrictor and dilator drugs in his experiments to achieve extreme blood flow rates. With flow measurements every 10 seconds, Burton achieved a blood flow range of 1cc/min/100 cc of tissue to 90cc/min/100cc. The normal range of blood flow for a subject under comfortable environmental conditions was determined to be between 15 and 40 cc/min/100cc of tissue. Burton explains that the degree of acclimatization to an environment also affects the minimum and maximum blood flow rates in fingers.

Burton found that the blood flow changes every second, so he correlated blood flow to the size of the finger volume pulse. He found that these fluctuations in blood flow are rhythmic in nature and are present in all the extremities of the body and are accompanied by cardiac acceleration and increase in blood pressure. Burton explains that the rhythms in blood flow are caused by the normal respiratory cycle and some of the constrictions in the blood flow might be in response to pain, startle or emotion. Burton points out that the fluctuations in blood flow is high during normal conditions and is dampened at extreme temperatures. Burton states that the regulation of body temperature can be achieved by adjusting the average blood flow value between the maximum and minimum values of fluctuation.

2.3.2 Greenfield et al. Finger Blood Flow Test

Greenfield, Shepherd and Whelan (1950) determined the proportions and the ranges of the hand blood flow that would pass through to the fingers. They conducted experiments on seven volunteers aged 19-32 years in three different environments. In one experiment, all volunteers were lightly clad in a room at 11.5-20^{o}C. In another, the volunteers were normally clad in a 20-29^{o}C room and in the third they were wrapped in blankets in a room at 26-30^{o}C with both calves and feet in a stirred water bath a 43^{o}C. Greenfield et.al measured the amount of blood flow flowing through the fingers by occluding the blood flow to the fingers with a rubber band in the left hand and comparing the hand blood flow results with and without the rubber band. They ensured that there was normal blood flow in the right hand under both the set of conditions.

Greenfield et.al reported that under normal conditions 46-82% (average 69%) of the total hand blood flow will pass through the fingers. Under cool conditions, it was reported that 19 to 64% of the total hand blood flow (average43.8%) and in hot conditions 27 to 58% of the total hand blood flow (average 44.5%) would pass through the fingers.

2.3.3 Zweifler et al. Finger Blood Flow Test

Zweifler et.al (1967) studied the relationship between digital blood flow and digital pulse volume. Ten normal subjects and ten patients suffering with scleroderma and Raynaud's phenomenon were chosen. Blood flow in the middle fingers of all the subjects was measured by the venous occlusion technique .Measurements of pulse and flow were made in casual, cool, heated and maximum dilatation. In the casual condition, the room temperature was 75^{o}F and the patients were lightly covered. In the cool condition, room temperature was 65^{o}F and the patients were lightly covered. In the heated condition, the patient covered from neck to toes with woolen

blankets was directly heated with heating pads until the oral temperature increased by atleast 0.5^{o}F. These measurements were done in a room temperature of 80^{o}F.The conditions for maximum dilatation experiment were similar to that of heated condition except that the pulse measurements were made after 10 minutes of direct warming of the hand with heating pads.

Zweifler et.al reported pulse volume values corrected for a unit of 5 ml finger volume and for pulse pressure as 5.1±2.1 ml/5ml/mmHg in cool conditions to 23.7±7.0 ml/5ml/mmHg in maximum dilatation conditions for normal subjects. For patients, the pulse volume values ranged from 5.0±3.9 ml/5ml/mmHg under casual conditions to 9.4±4.5 ml/5ml/mmHg in maximum dilatation conditions. Zweifler achieved a blood flow of 0.67±0.56 ml/5ml/min in cool conditions, 1.11±0.84 ml/5ml/min in casual conditions and 2.16±0.66 ml/5ml/min in heated conditions for normal subjects. For patients suffering from Raynaud's disease, he obtained a blood flow of 0.35±0.21 ml/5ml/mm Hg under casual conditions and a flow of 0.75±0.42 ml/5ml/min in heated conditions.

Zweifler et.al observed that within an individual, changes in finger blood flow were found to be directly paralleled by the size of the finger volume under different conditions. However, the pulse volume- blood flow relationship differed widely among individuals although the scatter was less for normal patients than those suffering from Raynaud's phenomenon. Zweifler et.al concludes that the pulse volume is a reliable indicator of the state of vascular bed as blood flow.

2.3.4 Coffman Finger Blood Flow Test

J.D.Coffman investigated the total and nutritional blood flow in the fingertip during total body cooling. Coffman measured the total blood flow rate in the finger by venous occlusion technique and the nutritional blood flow by the disappearance rate of a radioactive isotope

($Na^{131}I$). Experiments were performed with the subjects lightly clothed, in a room at 28.3^{o}C for 1 hr and then repeated after 1 hr in a room at 20^{o}C.Experiments were also conducted with intra-arterial infusion of norepinephrine.

Coffman measured the fingertip blood flow after 1 hr of body warming on an average to be 59.7 ml /min/100g and after 1 hr of cooling to be 32.7 ml /min/100g.Coffman measured the disappearance rates of $Na^{131}I$ to be 3.7 min in the warm room and 5.6 min in the cool room. These disappearance rates were then converted into estimated nutritional flow which is 10 ml /min/100g in warm room and 7 .3 ml /min/100g in cool room. During the norepinephrine infusion, fingertip blood flow averaged 34.8 ml and the disappearance rate was 8.0 minutes compared to values of 72.8 ml and 5.2 minutes during the control period (before norepinephrine infusion).

Coffman concludes that during body cooling, total blood flow to the finger decreases with no major reduction in the nutritional blood flow. Coffman estimates the nutritional blood flow in the fingertip to be 10-20% of the total blood flow.

2.3.5 Cooke et al. Finger Blood Flow Test

This study determined the effect of gender differences in the local or central control of cutaneous blood flow that accounted for increased incidence of Raynaud's disease in women. Cooke et.al (1990) conducted experiments on 23 men and 26 women and measured hand blood flow, finger blood flow and skin perfusion. Hand blood flow in the volunteers was measured using volume plethysmography, finger blood flow using mercury strain-gauge plethysmography and skin perfusion using laser Doppler spectroscopy. Cooke et.al conducted experiments to establish the following:

a) Gender differences in basal cutaneous blood flow

b) Gender differences in the interaction of central and local control

c) Gender differences in local control

d) Gender differences in central control

e) Hormonal effects on control of cutaneous blood flow.

Cooke et.al reported that the basal cutaneous blood flow in men exceeded that of women. The hand blood flow in men was measured to be 12.1±2.0 ml/100ml/min whereas in women, it was 6.2±1.5 ml/100ml/min. Finger blood flow was 16.9±4.8 ml/100ml/min in men whereas it was 7.7±1.8 ml/100ml/min in women. Both the male and female volunteers showed the same response to the local warming/cooling of the hand. Deep inhalation reduced blood flow under normal conditions for men and under warm conditions for women. Mental stress caused increase in blood flow in normal conditions for women and cool conditions for men. No changes in blood flow were observed in females when the experiments were conducted throughout the month. Cooke et.al concludes that the gender differences in the control of hand blood flow would have been the reason behind increased incidence of Raynaud's disease in women.

2.4 Finger Thermal Models

Finger Thermal Models provide a harmless way to evaluate human responses at different environmental conditions. Finger Thermal Models can also be used to judge the effect of gloves on fingers in cold temperatures. For example, Shitzer et al. (1991, 1997) developed a one dimensional and a two dimensional model and predicted the effectiveness of these finger models by comparing the model results with experimental data. Karaki et al. (2013) extended Salloum's idea of arterial representation to fingers. Karaki included the effect of arteriovenous anastomoses (AVA) in the human thermal system. The above mentioned models have been discussed in this section.

2.4.1 Shitzer 1-D Model

Shitzer et al. (1991) developed a one dimensional finger model to predict the endurance times of human fingers to cold temperatures. Only conduction, convection and heat exchange at the base of the cylinder (connection between finger and hand) were considered in the 1D heat transfer model. These assumptions give axial temperature variations only. Shitzer et al. assumed uniform metabolic heat generation, uniform thermophysical properties and no cold induced vasodilatation (CIVD) in the model. Equation (2-11) represents the one dimensional transient energy balance equation used.

$$\rho c \frac{\partial T}{\partial t} = \kappa \frac{\partial^2 T}{\partial z^2} + q - \frac{ph(T - T_0)}{A} \qquad (2\text{-}11)$$

In the above equation , ρ is the density, c is the specific heat, T is the temperature, t is time, κ is thermal conductivity, z is the axial coordinate, p is the circumference of the cylinder, h is the heat transfer coefficient, A is the cross sectional area of the cylinder and T_0 is the environmental temperature.

The above equation was subjected to initial temperature and boundary convection conditions. Shitzer used orthogonal integral transformations to solve the energy balance equations in order to compute the temperatures in the model.

Shitzer et.al compared his model to the Santee et al. (1990) experiments of light duty gloves (only sitting tests). Shitzer's model predictions compared well with the experimental results. Shitzer's one dimensional model was used to study the digit behavior at different insulation values, different digit lengths, different digit diameters, different environmental temperatures. Shitzer et al. also estimated the endurance times of fingers exposed to cold weather with the help of the present 1D model.

2.4.2 Shitzer 2-D Model

Shitzer et al. (1997) developed a two dimensional finger model which considers heat transfer in radial and axial directions. They also included metabolic heat generation, heat transport by blood perfusion, heat exchange between the tissue and blood vessels and arteriovenous exchange.

The 2 D finger model is a right angle cylinder of 8cm length and 1.5 cm diameter. Blood vessels are represented in the present model with one artery and vein. The size of these blood vessels is set such that they represent the effects of all the blood vessels in the finger. The diameter of the artery is 0.2 cm and that of the vein is 0.3 cm. The finger model is subdivided into four cylindrical layers- core, muscle, fat and skin. Each layer is further subdivided in the radial and axial directions. Energy balance equations are written for the tissue, artery and vein and mass conservation equations for artery and vein:

Tissue

$$\rho c \frac{\partial T^*}{\partial t^*} = \kappa \left[\frac{1}{r^*} \frac{\partial}{\partial r^*} \left(r^* \frac{\partial T^*}{\partial r^*} \right) + \frac{\partial^2 T^*}{\partial z^{*2}} \right] + q_m + w_b c_b (T_a - T) + u_a (T_a - T) + u_v (T_v - T) \qquad (2\text{-}12)$$

In the above equation, the term on the left hand side represents the rate of change of stored energy and the terms on the right hand side represents radial, axial heat conduction, metabolic heat generation, blood perfusion, heat exchange with the artery and vein.

Artery

$$M_a c_b \frac{d\bar{T}_a^*}{dt^*} = m_{a,in} c_b T^*_{a,in} - m_{a,out} c_b T^*_{a,out} + \int u_a (T^* - T_a^*) dv + h_{av} (T^*_v - T_a) - \int w_b c_b T_a^* dv \qquad (2\text{-}13)$$

$$m_{a,in} = m_{a,out} + \int w_b dv \qquad (2\text{-}14)$$

Vein

$$M_v c_b \frac{d\bar{T}_v^*}{dt^*} = m_{v,in} c_b T^*_{v,in} - m_{v,out} c_b T^*_{v,out} + \int u_v (T^* - T_v^*) dv + h_{av} (T^*_a - T_v^*) \qquad (2\text{-}15)$$

$$- \int w_b c_b \, T^* dv$$

$$m_{v,in} = m_{v,out} - \int w_b dv \qquad (2\text{-}16)$$

In the above heat balance equations for artery and vein, the left hand side represents the average amount of blood stored in blood in these vessels at any instant. The terms on the right hand side represent the enthalpy flux into and out of the control volume, heat transfer with the tissue, countercurrent heat exchange between the artery and vein and the last term is the drainage into/collection from cylinder during perfusion.

Shitzer et al. solved the above energy balance equations using initial and boundary heat transfer conditions. Then the equations are numerically solved by finite difference method.

Shitzer's two dimensional model predictions were compared with the model predictions of Shitzer et al. (1991) one dimensional finger model with the same set of parameters and boundary conditions. The two models were found to compare well. Shitzer's 2D model was used to estimate finger temperatures for gloved hand and bare hand at different environmental conditions, and steady state temperature distribution in the model with varying axial divisions.

2.4.3 Ghaddar Model

Karaki et al. (2012) improved Salloum (2007) segmental bioheat model to predict the human responses as well as the blood flow rates in peripheral body segments in transient environments. Karaki increased the number of body segments in Salloum's model by adding ten fingers to the model. These fingers were modeled like most other body segments with a core, skin, artery, deep vein and superficial vein.

Karaki et al. achieved better blood flow calculations by updating the thermoregulatory equation for the cardiac output proposed by Fu (1995). As blood flow was found to vary at higher core temperatures (unlike in Fu's model where blood flow was constant after a core temperature of 37.2^{o}C), the higher margin for the core temperature in the Fu's equation has been modified (changed from 37.2^{o}C to 41^{o}C) to include these changes in blood flow. Salloum's model was not applicable to changes in blood flow conditions due to the use of constant arterial radii. Karaki and Ghaddar introduced a correction to the arterial radii which depends on the cardiac output to account for the constant change in blood flow.

Karaki et al. developed finger AVA model from the existing Takemori et al. (1995) model considering an exponential way to define the maximum skin blood flow. The amount of blood flow to the finger was also defined differently from the model of Takemori et al. Karaki and Ghaddar used energy balance equations defined by Salloum (2007) for core, skin, artery, deep vein and superficial vein in each body segment. Energy balance equation for the superficial vein:

Superficial vein

$$C_{bl,v,s}\frac{dT_{bl,v,s}}{dt} = -\sum_{veins} h_{vein,s}A_{vein,s}(T_{bl,v,s} - T_{sk}) + m_{v,s}c_{bl}(T_{bl,v,s,adjacent} - T_{bl,v,s}) + m_{perfusion,sk}\,c_{bl}(T_{sk} - T_{bl,v,s}) + m_{AVA}\,c_{bl}(T_{bl,a} - T_{bl,v,s}) \quad (2\text{-}17)$$

The first term on the right hand side represents heat transfer between the vein and the skin, second term is the convective heat flow through the superficial vein, third terms represents the heat flow through perfusion and the last term is the direct heat transfer by AVA directly from the artery of the segment to the superficial vein.

Karaki et al. determined the temperature distribution within the system with the help of these energy balance equations. Karaki et al. also updated the blood flow at each time step using

these energy balance equations. Karaki compared his model simulation results with experimental published data and found that they were in good agreement.

Chapter 3 - Finger Model Development

The objective of this research is to develop a human finger model which interacts with the surroundings, provides accurate responses and which can be easily modified for further developments. Finite element techniques help us achieve the required detail and flexibility mentioned above. Finite element techniques discretize the finger into small, three- dimensional elements. Each element represents either a bone or skin in the finger model. The circulatory system is modeled using one- dimensional blood vessel elements. Conservation of mass, momentum and energy equations are used to develop a set of algebraic equations that can be solved for the unknown quantities e.g. pressure and temperature distribution within the model. Vasomotor and sudomotor responses are also used which control the skin blood flow and sweat rate in the finger model depending on the skin and core temperatures. This chapter provides a detailed description of the geometry, passive system and control equations as implemented in this finger model.

3.1 Geometry

In this section, a finger model is developed with the help of finite element techniques along with blood flow through the model to represent the real human finger as accurately as possible.

3.1.1 Tissues

The finger is modeled as cylinder with a hemispherical cap representing the fingertip. The finger is assumed to be a bone core enclosed within the skin layer. The radius of the finger is assumed to be 1.2cm and the length as 10.2 cm (both calculated from actual measurements).As already mentioned, finite element techniques were used to divide the finger into a number of

small three dimensional elements. The finger is divided radially, angularly and axially as shown in Figure 3.1. The number of divisions in each direction (for cylinder section of the finger model) is presented in Table 3.1.

Table 3.1 Finger Model Grid Generation

Direction	Number of Divisions
Radial	2
Axial	3
Angular	4

The fingertip in the model is divided into two concentric shells and four angular parts. The cylinder section of the finger model is constructed from triangular and rectangular three dimensional elements, similar to Smith's Model (Smith 1991). The fingertip is comprised of spherical elements.

The inner shell in the cylinder section as well as in the fingertip represents the bone and is 0.8cm in radius. The bone shell is surrounded by the skin layer which is 0.4cm thick. The axial divisions are each of 3 cm thick. The tissue properties in the finger Model are listed in Table 3.2 (Shitzer et.al 1997).

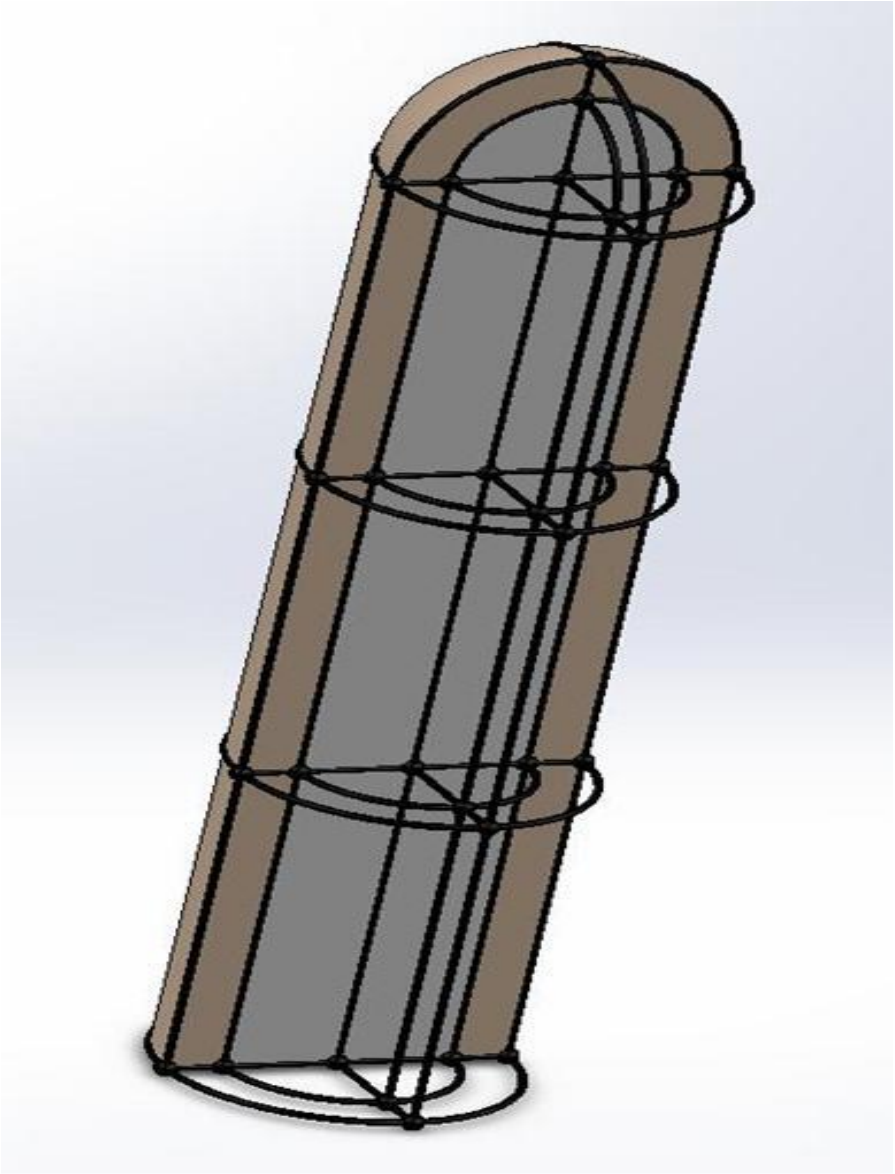

Figure 3.1 Finger with Radial, Axial and Angular Divisions

Table 3.2 Tissue Properties

Tissue	Density (kg/m^3)	Thermal Conductivity (W/mK)	Specific Heat(J/kgK)	Perfusion
Bone	1418	2.21	2094	0
Skin	1200	0.37	3391	0.2
Blood	1100	0.5	3300	1.0

3.1.2 Circulatory System

The circulatory system of the real human finger consists of two blood vessels carrying blood into the finger – radial and ulnar artery. The blood flowing into the finger then gets distributed throughout the finger with the help of capillaries. The blood is then carried out of the finger through two veins- radial and ulnar vein.

In this model, blood flows into the finger through two arteries, each on either side of the bone core. Blood circulates to the skin tissue at each axial level through arterioles, and at the skin surface, the blood returns to the central vein through venules. Blood flows to the fingertip through the two central arteries, and at the tip, the blood is distributed into superficial veins and central vein through which the blood returns. Blood flowing through the superficial vein returns to the central vein at the base of the finger through venules, and the blood flows out of the finger. Figures 3.2 and 3.3 illustrate the blood vessel distribution in the finger model.

The blood vessels in this model are represented as circular tubes and are located between each three dimensional elements, and run parallel to the edges of each tissue element. However, there is no blood flow in the bone shell. The blood flow data for a real human finger was presented in the experimental data of Burton (1939), Greenfield et al. (1951), Zweifler et al. (1967), Coffman (1972) and Cooke et al. (1990). Apart from the finger blood flow data presented by the aforementioned authors, Smith (1991) hand blood flow rates were also used to obtain

appropriate blood flow rates for the current finger model as Smith model data will be used as input for temperature calculations in the present model. Table 3.3 represents the blood flow in the present 3D finger model. The blood vessel radii for the present model have been obtained from this blood flow information. Blood vessel radii for the current model are shown in Tables 3.4 and 3.5.

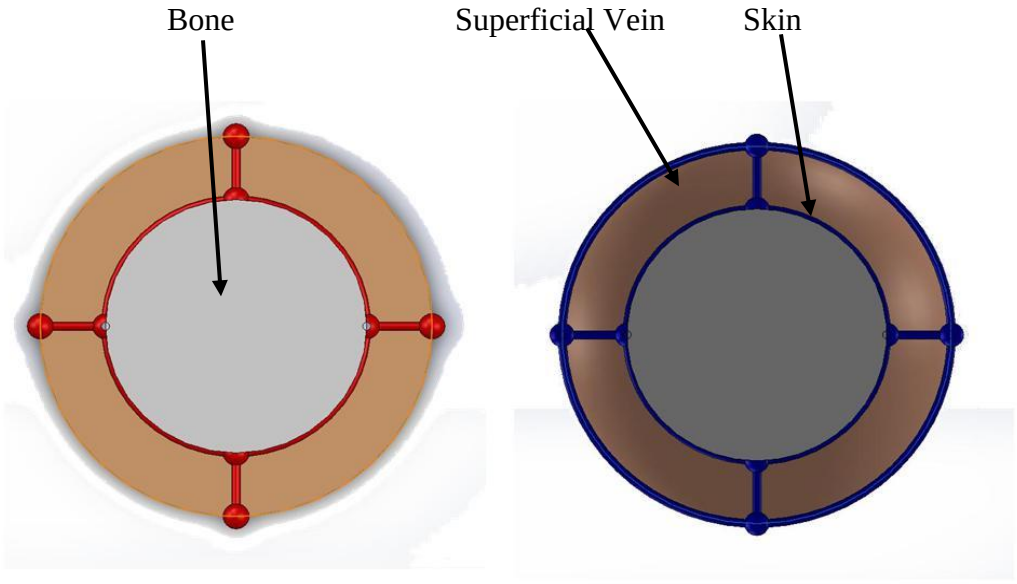

Figure 3.2 Top View of the Arterial and Venous Blood Vessel Network in the Finger Model

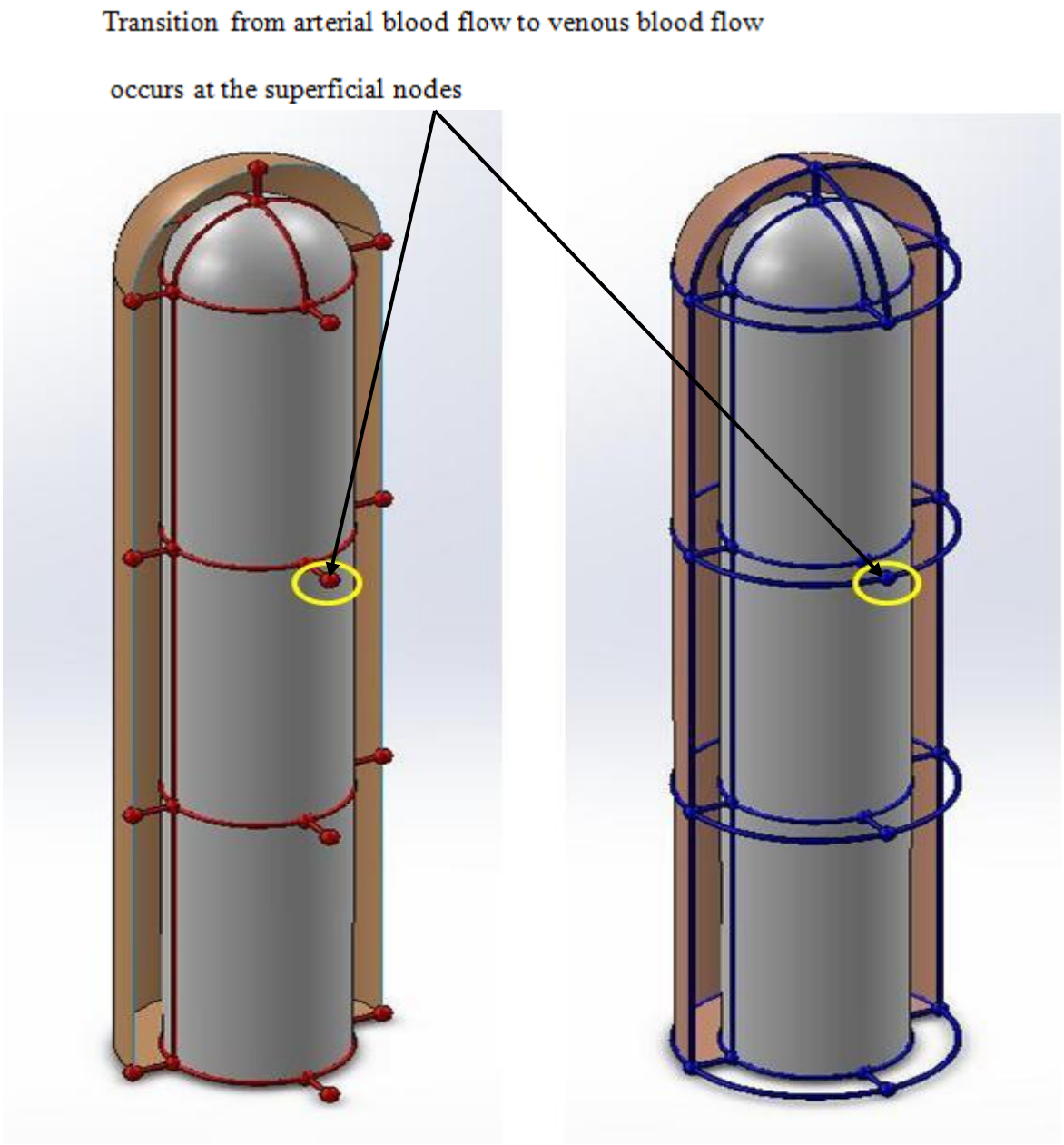

Figure 3.3 Cross-Sectional View of the Arterial and Venous Blood Vessel Network in the Finger Model

Table 3.3 Blood Flow data in The Finger Model

Condition	Blood Flow (cm3/hr)
Cold	100±50
Neutral	300±50
Hot	600±50

Table 3.4 Blood Vessel Radii (cm) in the Finger Model

Type of Blood Vessel	Artery	Vein
Connecting Blood Vessel in Fingertip	0.02941	0.00622-0.00913
Circular Blood Vessel in Fingertip	0.04437	0.08874
Deep Blood Vessels	0.05882	0.11765
Other Blood Vessels	0.01747	0.03493

Table 3.5 Range of Superficial Vein radii in different temperatures

Superficial Veins(cm)	Basal	Max. Constrict	Max. Dilate
	0.04	0.032	0.047

3.2 Passive System

Heat Transfer in the finger is affected by the environmental conditions and the temperature distribution in the finger. Blood flow in the finger is a pressure driven model similar to the model used in Smith and it has a dominant effect on the temperature distribution in the finger. Blood flow in the finger was assumed to be one dimensional in axial direction, steady, laminar, incompressible, axisymmetric and fully developed as was done by Smith (1991).

3.2.1 Tissue Energy Balance Equation

Temperature distribution in the tissue and blood vessels are determined by solving the energy balance equations for the tissue and the blood vessel. George Fu (1995) considered perfusion in the blood vessels in his model which is an extension to Smith Model (1991). According to Fu's Model, energy balance equation for any tissue element is:

$$\rho C_p\left(\frac{\partial T}{\partial t}\right) = \kappa\nabla.\nabla T + q''' + w_b\rho_b C_{p,b}(T_a - T_v) + q_a + q_v + \alpha q_{res} \qquad (3\text{-}1)$$

The above Equation (3-1) represents that the rate of heat storage in any tissue element is the summation of the heat conduction in the tissue, internal heat generation per unit volume, heat transferred due to perfusion, heat transferred from the arterial blood to tissue and heat transferred from the venous blood to tissue. The last term in the equation represents the heat transferred to the tissue from the respiratory system which is ignored in our study for temperature distribution in finger.

Internal Heat generation (q''') is assumed to be a combination of heat produced due to basal metabolism and voluntary physical activity. Shivering was not considered in our model, as our finger was modeled without any muscle tissue.

$$q''' = M_{basal} + M_{activity} \qquad (3\text{-}2)$$

Basal Metabolic Rates in each tissue element is shown in Table 3.5. (Shitzer et.al 1997)

Table 3.6 Basal Metabolic Rates in Tissue

Tissue	Basal Metabolic Heat Generation rate per unit volume(W/m^3)
Bone	170
Skin	250

3.2.2 Blood Vessel Energy Balance Equation

Similar to Smith's (1991) equation, the blood vessel energy balance equation for our model is

$$\rho_b C_{p,b} \left(\frac{\partial T_b}{\partial t}\right) = K_b \left(\frac{d^2 T_b}{dz^2}\right) - \rho_b C_{p,b} v_{bl} \left(\frac{dT_b}{dz}\right) \qquad (3\text{-}3)$$

assuming that the temperature varies only in the axial direction and constant thermal properties for blood such as specific heat $C_{p,b}$, density ρ_b and thermal conductivity K_b. The Equation (3-3) represents the rate of heat storage in a blood vessel due to conductive heat transfer and convective heat transfer due to the bulk motion of blood. In the above Equation, v_{bl} represents the mean blood velocity in the blood vessel elements.

3.2.3 Volumetric Blood Flow

The mean blood velocity (v_{bl}) is determined by the momentum equation,

$$v_{bl} = - \left[\frac{r_o^2}{8\mu}\right] \frac{dP_b}{dz} \qquad (3\text{-}4)$$

where dP_b/dz is the pressure gradient in the axial direction, μ represents the blood viscosity and r_o represents the blood vessel radii.

The blood vessel radii in this model changes according to the body thermal state i.e. body core temperature and body skin temperature. Control equation for the blood vessel radii is presented in Section 3.3.

Volumetric blood flow (V_{bl}) in each blood vessel element is calculated by multiplying the Equation (3-4) by the cross sectional area normal to the direction of flow, πr_o^2.

$$V_{bl} = - \left[\frac{\pi r_o^4}{8\mu}\right] \left(\frac{dP_b}{dz}\right) \qquad (3\text{-}5)$$

3.2.4 Pressure Distribution

The pressure distribution for the blood vessel network is determined by applying the conservation of mass principle to the blood flow. The below Equation represents the same:

$$\frac{dv_{bl}}{dz} = 0; \qquad (3\text{-}6)$$

Substituting the expression for mean blood velocity from Equation (3-4), the conservation of mass equation becomes:

$$- [\frac{r_o^2}{8\mu}] (\frac{d^2 P_b}{dz^2}) = 0 \qquad (3\text{-}7)$$

Galerkin Method of Weighted Residual is applied to the Equations (3-1), (3-3) and (3-7) to determine the pressure and temperature distribution in the blood vessel and tissue elements. The solution method will be discussed in detail in the next chapter.

3.3 Control System Equations

Thermal response in the human body is controlled by different mechanisms. Vasomotor mechanism controls the blood flow through the human body at different environmental temperatures. For example: In hot temperatures as body temperature rises, the blood flow in the human body increases to maintain temperatures within safe limits. In extreme cold temperatures as body temperature drops, the blood flow decreases considerably to maintain thermal balance in critical parts of the human body. Sudomotor mechanism in the human body controls the sweat rate. Shivering response increases the metabolic rate in the human body at low temperatures to increase the body temperature.

Hypothermia is also an important mechanism in the human body and is also considered fatal. When the body core temperature starts decreasing, the body starts shutting off blood to its

extremities in order to stay alive. Once the body core temperature falls beyond a certain limit, the human does not live any longer.

In the current model, only vasomotor and sudomotor mechanisms were considered. Shivering was not considered in the present study as there is no muscle in the model. Smith (1991) developed detailed control system equations for vasomotor and sudomotor response. Smith considered body core and skin temperatures to play a dominant role in determining these responses. Smith's vasomotor response has been modified to include the effect of hypothermia in humans.

3.3.1 Vasomotor response

Smith's (1991) vasomotor response is based on the assumption that the body undergoes maximum vasodilation when the body core temperature (T_{core}) is more than 37.2^{o}C and is in a state of maximum vasoconstriction when the body skin temperature (T_{skin}) is less than 10.7^{o}C. According to Smith (1991), the human would not survive if the body core temperature becomes less than 33^{o}C. The blood flow to the extremities is assumed to reduce when the body core temperature falls below 35 ^{o}C. Skin blood vessel radii at basal, vasodilation and vasoconstriction are calculated based on the blood flow at the corresponding conditions (Table 3.3).

Table 3.7 Condition for skin blood vessel radii at high temperatures

Radii	Temperature constraint	Calculation
$r_{o,dil}$	$T_{core} <= 36.8$	$r_{o,basal}$
	$T_{core} > 36.8 \;\&\&\; T_{core} < 37.2$	$((T_{core} - 36.8)/(37.2-36.8))* (r_{o,maxdil} - r_{o,basal}) + rbv$
	$T_{core} >= 37.2$	$r_{o,maxdil}$

$r_{o,basal}$ is the blood vessel radii at basal state and $r_{o,maxdil}$ is blood vessel radii at maximum vasodilation state .

Table 3.8 Condition for skin blood vessel radii at low temperatures

Radii	Temperature constraint	Calculation
$r_{o,con}$	$T_{skin} <= 10.7$	$r_{o,maxcon}$
	$T_{skin} >10.7 \&\& T_{skin} < 33.7$	$((T_{skin} - 33.7)/(33.7-10.7))* (r_{o,basal} -rmcv) + r_{o,maxcon}$;
	$T_{skin} >= 33.7$	$r_{o,basal}$

$r_{o,maxcon}$ is the blood vessel radii at maximum vasoconstriction state .

$r_{o,dil}$ and $r_{o,con}$ are skin blood vessel radii including any effects of vasodilation and vasoconstriction.

$$\text{Original Blood vessel radii (r1)} = \frac{r_{o,dil} * r_{o,con}}{r_{o,basal}} ; \qquad (3\text{-}8)$$

Condition for Hypothermia

$$r_o = \begin{cases} r1 * \dfrac{(T_{core} - 33)}{(35 - 33)} & \text{for } T_{core} < 35 \\ r1 \end{cases} \qquad (3\text{-}9)$$

The final blood vessel radii (r_o) is calculated by applying the hypothermia condition (Equation (3-9)) to the original blood vessel radii (Equation (3-8)) obtained using Smith's vasomotor responses.

3.3.2 Sudomotor response

Sweating threshold, T_{sweat} is one of the controlling factor in the sudomotor response for the finger. Sweating takes place if the body core temperature (T_{core}) exceeds either T_{sweat} or 37.1°C. Sweating threshold (T_{sweat}) is a function of skin temperature (T_{skin}).

$$T_{sweat} = \begin{cases} 42.084 - 0.15833\, T_{skin} & \text{for } T_{skin} < 33.0^{o}C \\ 36.85 & \text{for } T_{skin} >= 33.0^{o}C \end{cases} \quad (3\text{-}10)$$

Sweat rate (m_{sw}) in the model is given by

$$m_{sw} = 45.8 + 739.4(T_{core} - T_{sweat}) \quad \text{in g/hr} \quad (3\text{-}11)$$

The maximum value for sweat rate is 696 g/hr. Sweat rate per unit surface area (m_{rsw}) is calculated by dividing the sweat rate with the total surface area ($A_{s,t}$) of the finger.

$$m_{rsw} = \frac{m_{sw}}{A_{s,t}} \quad (3\text{-}12)$$

Sweat rate per unit surface area is used in the calculation of P_{skin} which in turn is used to calculate the evaporative heat loss in the finger model which will be discussed in detail in the next chapter.

Chapter 4 - Solution Method

4.1 Finite Element Method

Thermal governing equations mentioned in Chapter 3 are solved numerically to determine the pressure distribution in blood vessels, temperature distribution in the blood vessels and tissues. Finite Elements Techniques offer a number of advantages over finite difference techniques as shown by Smith (1991) thus Finite Elements has been used to develop a solution.

4.1.1 Shape Functions of Finger Model

The Finger Model is made up of triangular, rectangular, spherical and one dimensional elements. The triangular, rectangular and one dimensional element are the same as those used in Smith Model (1991). The finger model consists of two additional types of spherical elements:

a) Four- node spherical elements forming the bone in the fingertip.

b) Six –node spherical elements forming the skin in the fingertip.

Nodes are located at the corners of these elements as shown in Figure 4.1. Nodes are numbered both locally and globally. In our Finger Model, the node numbering starts from the fingertip. Shape Functions are derived for each element shape using the same method as outlined in Segerlind (1984). Finite Element Techniques use shape functions to define the unknown quantity i.e.; pressure and temperature at any location within an element. The shape functions of all the elements forming the finger model are as follows:

a) Triangular Elements

i. $N_1 = \dfrac{(r*\theta*z)}{(\Delta r*\Delta\theta*\Delta z)}$;

ii. $N_2 = \dfrac{(r*(\Delta\theta - \theta)*z)}{(\Delta r*\Delta\theta*\Delta z)}$;

iii. $N_3 = \dfrac{\left(\left(\Delta r - r\right) * \Delta\theta * z\right)}{\left(\Delta r * \Delta\theta * \Delta z\right)};$

iv. $N_4 = \dfrac{\left(r * \theta * \left(\Delta z - z\right)\right)}{\left(\Delta r * \Delta\theta * \Delta z\right)};$

v. $N_5 = \dfrac{\left(r * \left(\Delta\theta - \theta\right) * \left(\Delta z - z\right)\right)}{\left(\Delta r * \Delta\theta * \Delta z\right)};$

vi. $N_6 = \dfrac{\left(\left(\Delta r - r\right) * \Delta\theta * \left(\Delta z - z\right)\right)}{\left(\Delta r * \Delta\theta * \Delta z\right)};$ *(4-1)*

b) Rectangular Elements

i. $N_1 = \dfrac{\left(\left(r - r_0\right) * \theta * z\right)}{\left(\Delta r * \Delta\theta * \Delta z\right)};$

ii. $N_2 = \dfrac{-\left(\left(r - r_0\right) * \left(\theta - \Delta\theta\right) * z\right)}{\left(\Delta r * \Delta\theta * \Delta z\right)};$

iii. $N_3 = \dfrac{\left(\left(r - \left(r_0 + \Delta r\right)\right) * \left(\theta - \Delta\theta\right) * z\right)}{\left(\Delta r * \Delta\theta * \Delta z\right)};$

iv. $N_4 = \dfrac{-\left(\left(r - \left(r_0 + \Delta r\right)\right) * \theta * z\right)}{\left(\Delta r * \Delta\theta * \Delta z\right)};$

v. $N_5 = \dfrac{-\left(\left(r - r_0\right) * \theta * \left(z - \Delta z\right)\right)}{\left(\Delta r * \Delta\theta * \Delta z\right)};$

vi. $N_6 = \dfrac{\left(\left(r - r_0\right) * \left(\theta - \Delta\theta\right) * \left(z - \Delta z\right)\right)}{\left(\Delta r * \Delta\theta * \Delta z\right)};$

vii. $N_7 = \dfrac{-\left(\left(r - \left(r_0 + \Delta r\right)\right) * \left(\theta - \Delta\theta\right) * \left(z - \Delta z\right)\right)}{\left(\Delta r * \Delta\theta * \Delta z\right)};$

viii. $N_8 = \frac{\left(\left(r-\left(r_0+\ \Delta r\right)\right)*\theta\ *\left(z-\ \Delta z\right)\right)}{\left(\Delta r*\Delta\theta*\Delta z\right)};$ *(4-2)*

c) One Dimensional Elements

i. $N_1 = \frac{\left(\Delta z\ -z\right)}{\Delta z};$

ii. $N_2 = \frac{z}{\Delta z};$ *(4-3)*

d) Spherical Elements(four-node)

i. $N_1 = \frac{(r*\ \theta\ *\phi)}{\left(\Delta r*\Delta\theta\ *\Delta\phi\right)};$

ii. $N_2 = \frac{(r*\left(\Delta\theta\ -\ \theta\right)*\ \phi)}{\left(\Delta r*\Delta\theta\ *\Delta\phi\right)};$

iii. $N_3 = \frac{(\left(\Delta r\ -r\right)*\ \Delta\theta\ *\ \Delta\phi)}{\left(\Delta r*\Delta\theta\ *\Delta\phi\right)};$

iv. $N_4 = \frac{(r*\ \Delta\theta\ *\left(\Delta\phi\ -\phi\right))}{\left(\Delta r*\Delta\theta\ *\Delta\phi\right)};$ *(4-4)*

e) Spherical Elements(six-node)

i. $N_1 = \frac{\left(r-\ r_0\right)*\ \theta*\phi}{\left(\ \Delta r*\Delta\theta\ *\Delta\phi\right)};$

ii. $N_2 = \frac{(\left(r-\ r_0\right)*\left(\Delta\theta\ -\theta\right)*\ \phi)}{\left(\Delta r*\Delta\theta\ *\Delta\phi\right)};$

iii. $N_3 = \frac{(\left(\left(r_0+\ \Delta r\right)-r\right)*\ \theta*\phi)}{\left(\Delta r*\Delta\theta\ *\Delta\phi\right)};$

iv. $N_4 = \frac{(\left(\left(r_0+\ \Delta r\right)-r\right)*\left(\Delta\theta\ -\theta\right)*\ \phi)}{\left(\Delta r*\Delta\theta\ *\Delta\phi\right)};$

v. $N_5 = \dfrac{(((r_0 + \Delta r) - r) * \Delta\theta * (\Delta\phi - \phi))}{(\Delta r * \Delta\theta * \Delta\phi)}$;

vi. $N_6 = \dfrac{((r - r_0) * \Delta\theta * (\Delta\phi - \phi))}{(\Delta r * \Delta\theta * \Delta\phi)}$; *(4-5)*

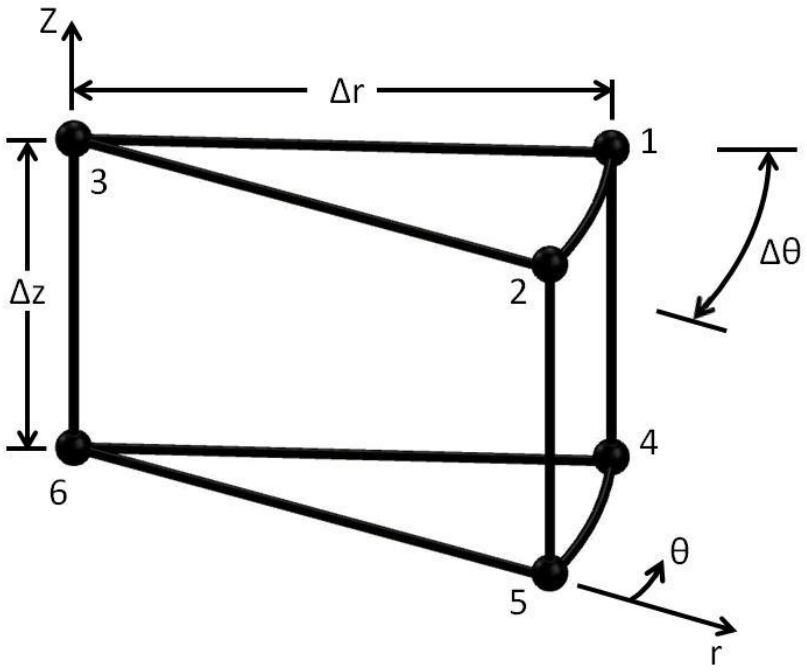

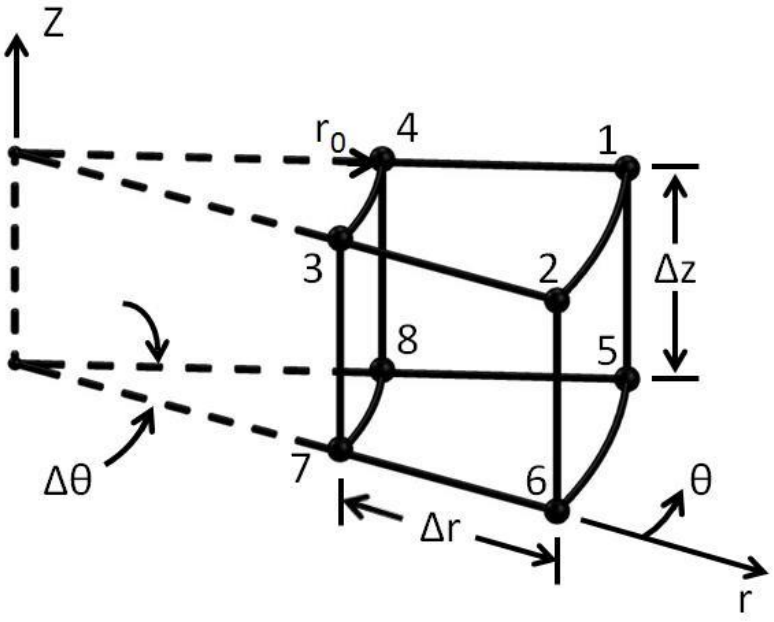
Z
r0
4
1
3
2
Δz
8
5
Δθ
7
6
θ
Δr
r

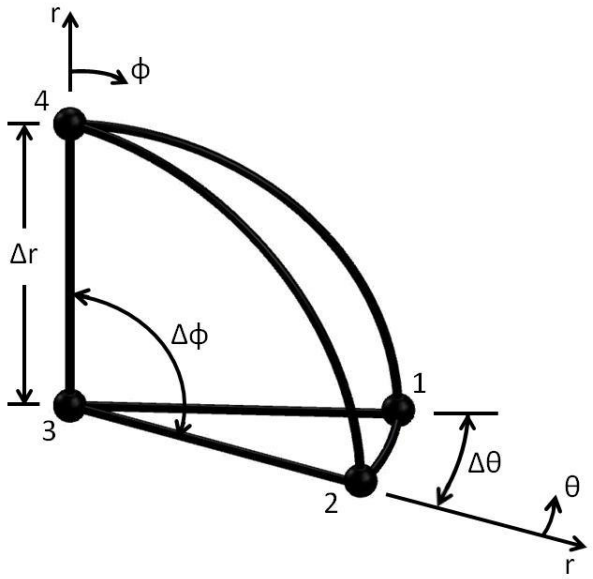
r
ϕ
4
Δr
Δϕ
1
3
Δθ
θ
2
r

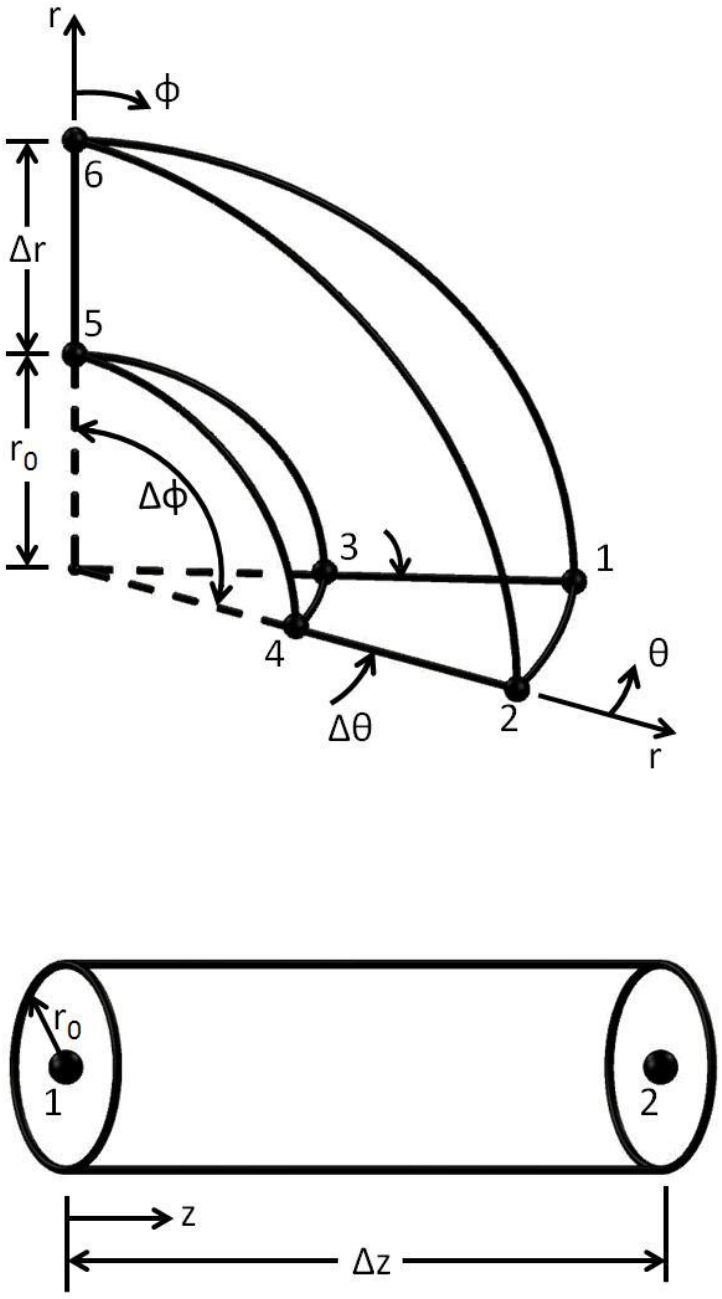

Figure 4.1 Element Shapes used in the Finger Model with Local Node Numbering

4.1.2 Application of Galerkin Method of Weighted Residual

Galerkin Method of weighted residual is used to solve the passive system equations presented in Chapter 3. Galerkin Method discretizes the governing equation which has first order or higher derivatives. The shape functions of each element are used as weighting functions in the integral. Application of Galerkin Method yields a system of linear simultaneous equations which can be solved for the desired unknown quantity. In this section, Galerkin Method is applied to Equations (3-1), (3-3), (3-7) to determine the temperature distribution in tissue, blood vessels and the pressure distribution in the blood vessels. As Smith (1991) has already discussed the application of Galerkin Method to determine the pressure distribution and temperature distribution in blood vessels in her thesis, the same won't be repeated here. In our discussion, Galerkin Method is applied to the four node and six node spherical elements and the resulting equations will be presented.

4.1.2.1 Pressure Distribution

Galerkin Method of Weighted Residual is applied to Equation (3-7) for each blood vessel element. This results in N linear simultaneous equations with N unknowns which are the nodal pressures. Here N represents the number of nodes used to model the circulatory system. The current model has an N of 51. Boundary conditions are imposed on the equations to solve for the pressure distribution in the finger Model. Detailed derivation of the N equations can be found in Smith's Thesis (1991).

4.1.2.2 Transient Temperature Distribution in Tissue

Passive System Equation (3-1) governs the temperature distribution in the tissue:

$$\rho C_p\left(\frac{\partial T}{\partial t}\right) = \kappa\nabla.\nabla T + q''' + w_b\rho_b C_{p,b}(T_a - T_v) + q_a + q_v + \alpha q_{res} \qquad (3\text{-}1)$$

Application of Galerkin Method yields:

$$\int_V [N]\left(\rho C_p\left(\frac{\partial T}{\partial t}\right) - \kappa\nabla.\nabla T - q''' - w_b\rho_b C_{p,b}(T_a - T_v) - q_a - q_v\right)dV = 0 \qquad (4\text{-}6)$$

In the above equation, [N] is 1-D array which contains shape functions of all the 3D elements in the finger model.

The last term in Equation (3-1) has been ignored as we do not consider respiratory term to determine the temperature distribution in the finger.

Green's First Theorem is applied to the second term ($\kappa\nabla.\nabla T$) in Equation (4-6) to reduce the order of integration. The resulting energy balance equation is:

$$\int_V \rho C_p [N]\left(\frac{\partial T}{\partial t}\right) dV + \int_V \kappa\nabla[N].\nabla T\, dV - \kappa\int_{As}[N](n.\nabla T)dAs - \int_V [N](q''' + q_p)\, dV -$$

$$\int_V [N](q_a + q_v)\, dV = 0 \qquad (4\text{-}7)$$

where ∇ is the gradient operator defined in spherical coordinates for spherical elements and defined in cylindrical coordinates (Smith 1991) for cylindrical elements.

Del in spherical coordinates:

$$\nabla = \frac{\partial}{\partial r}\vec{r} + \frac{1}{r}\frac{\partial}{\partial\theta}\vec{\theta} + \frac{1}{r\sin\theta}\frac{\partial}{\partial\phi}\vec{\phi} \qquad (4\text{-}8)$$

In Equation (4-7), $q_p = w_b\rho_b C_{p,b}(T_a - T_v)$ is the heat transferred to the tissue due to perfusion.*(4-9)*

Equation (4-7) is integrated for all the three dimensional elements in the present model. Only spherical elements were considered for our discussion.

The first term in Equation (4-7) contains the term $(\frac{\partial T}{\partial t})$ which is integrated using lumped formulation to define the spatial variation as discussed in Smith (1991) Thesis.

Let $(\frac{\partial T}{\partial t}) = [N^*]^T\{\dot{T}\}^e$ where [N*] is the vertical array of new shape functions and $\{\dot{T}\}^e=[\dot{T}_1\dot{T}_2\dot{T}_3...\dot{T}_n]^T$ where n is the number of nodes in the element.

For a four node spherical elements, the centroid coordinates are located at (r_c, θ_c, ϕ_c) where

$$r_c = 3*\frac{\Delta r}{4} \quad (4\text{-}10)$$

$$\theta_c = 1 \quad (4\text{-}11)$$

$$\phi_c = \frac{\Delta\phi}{2} \quad (4\text{-}12)$$

For a six node spherical elements, the centroid coordinates (r_c, θ_c, ϕ_c) are:

$$r_c = \frac{3((r_0+\Delta r)^4 - r_0^{\,4})}{4((r_0+\Delta r)^3 - r_0^{\,3})} \quad (4\text{-}13)$$

$$\theta_c = 1 \quad (4\text{-}14)$$

$$\phi_c = \frac{\Delta\phi}{2} \quad (4\text{-}15)$$

where r_0 is the radii of the inner spherical elements forming the bone.

Step functions are used to define the new shape functions for each element shape. These step functions are functions of the centroids of each element shape. The step functions are:

$$h(r-r_c) = 0 \text{ for } r \le r_c \text{ and } h(r-r_c) = 1 \text{ for } r > r_c \quad (4\text{-}16)$$

$$h(\theta-\theta_c) = 0 \text{ for } \theta \le \theta_c \text{ and } h(\theta-\theta_c) = 1 \text{ for } \theta > \theta_c \quad (4\text{-}17)$$

$$h(\phi-\phi_c) = 0 \text{ for } \phi \le \phi_c \text{ and } h(\phi-\phi_c) = 1 \text{ for } \phi > \phi_c \quad (4\text{-}18)$$

The new shape functions for the four node spherical elements are:

$$i. \quad N_1^* = h(r-r_c)^* h(\theta-\theta_c)\ ^*h(\phi-\phi_c);$$

$$ii. \quad N_2^* = h(r-r_c)^*(1-h(\theta-\theta_c))^* h(\phi-\phi_c);$$

$$iii. \quad N_3^* = (1-h(r-r_c));$$

$$iv. \quad N_4^* = h(r-r_c)\ ^*(1-h(\phi-\phi_c)); \qquad (4\text{-}19a)$$

The new shape functions for the six node spherical elements are:

$$i. \quad N_1^* = h(r-r_c)^* h(\theta-\theta_c)\ ^* h(\phi-\phi_c);$$

$$ii. \quad N_2^* = h(r-r_c)^*(1-h\ (\theta-\theta_c))^* h(\phi-\phi_c);$$

$$iii. \quad N_3^* = (1-h(r-r_c))^* h(\theta-\theta_c)^* h(\phi-\phi_c);$$

$$iv. \quad N_4^* = (1-h(r-r_c))^*(1-h(\theta-\theta_c))^* h(\phi-\phi_c);$$

$$v. \quad N_5^* = (1-h(r-r_c))^*(1-h(\phi-\phi_c)));$$

$$vi. \quad N_6^* = (h(r-r_c))^*(1-h(\phi-\phi_c)); \qquad (4\text{-}19b)$$

After substitution of the new shape functions, the first term in Equation (4-7) becomes

$$\int_V \rho C_p\,[N]\,\left(\frac{\partial T}{\partial t}\right) dV = \rho C_p \int_0^{\Delta r}\int_0^{\pi/2}\int_0^{\pi/2} [N^*]\,[N^*]^T r^2 dr\sin\theta d\theta d\phi \qquad (4\text{-}20a)$$

$$\int_V \rho C_p\,[N]\,\left(\frac{\partial T}{\partial t}\right) dV = \rho C_p \int_{r0}^{\Delta r+r0}\int_0^{\pi/2}\int_0^{\pi/2} [N^*]\,[N^*]^T r^2 dr\sin\theta d\theta d\phi \qquad (4\text{-}20b)$$

Equation numbers following with a ‘a’ apply for the four node spherical elements while those followed by a ‘b’ apply for the six node spherical elements.

The second term in Equation (4-7) can be solved by direct substitution of shape functions and temperature using:

$$T = [N]^T\{T\}^e$$

where $\{T\}^e = [T_1 T_2 T_3 \ldots T_n]^T$

$$\int_V \kappa \nabla[N].\ \nabla T\, dV = \kappa \int_0^{\Delta r}\int_0^{\Delta\theta}\int_0^{\Delta\phi} \nabla[N].\ \nabla[N]^T r^2 dr\sin\theta d\theta d\phi \qquad (4\text{-}21a)$$

$$\int_V \kappa \nabla[N].\ \nabla T\, dV = \kappa \int_{r0}^{\Delta r+r0} \int_0^{\Delta\Theta} \int_0^{\Delta\phi} \nabla[N].\ \nabla[N]^T\, r^2 dr \sin\theta d\theta d\phi \qquad (4\text{-}21b)$$

The third term in Equation (4-7) is solved by applying the boundary conditions for each element. For the exposed element surfaces:

$$n.\ \nabla T = h_c(T_{air} - T) + h_r(T_{sur} - T) + m_m'' h_{fg}\, dA_s \qquad (4\text{-}22)$$

The first term in Equation (4-22) represents the convective heat loss from the element surface to the surroundings. The second term in the above equation represents the radiative heat loss from the element surface to the surroundings and the last term represents the evaporative heat loss to the surroundings. h_c and h_r represent the convective and radiative heat transfer coefficients , h_{fg} represents the latent heat of vaporization. T_{air} and T_{sur} are the ambient and radiant temperatures of the surroundings. A_s is the area of the element surface exposed to the surroundings. m_m'' is the rate at which moisture evaporates to the surroundings.

The convective heat loss and the radiative heat loss can be calculated by substituting the values of h_c, h_r, T_{air}, T_{sur} which are the input conditions for the finger model. Evaporative Heat loss in the present Model has been calculated using Jones Model (1993a) which has been presented in detail in Appendix A.

The forth term in Equation (4-7) can be solved by direct substitution of shape functions, and with the assumptions that the metabolic heat generation and perfusion are uniform within each tissue element.

$$\int_V [N](q''' + q_p)\, dV = (q''' + q_p) \int_0^{\Delta r} \int_0^{\Delta\theta} \int_0^{\Delta\phi} \nabla[N] r^2 dr \sin\theta d\theta d\phi \qquad (4\text{-}23a)$$

$$\int_V [N](q''' + q_p)\, dV = (q''' + q_p) \int_{r0}^{\Delta r+r0} \int_0^{\Delta\theta} \int_0^{\Delta\phi} \nabla[N] r^2 dr \sin\theta d\theta d\phi \qquad (4\text{-}23b)$$

The last term in Equation (4-7) represents the convective heat exchange with the surrounding blood vessels (arteries and veins) (edge convection condition page 241 of Finite Element Analysis). Amount of heat lost to the surrounding artery (q_a) is given by:

$$q_a=2\pi r_a h_a(T_a-T) \qquad (4\text{-}24)$$

Amount of heat lost to the surrounding vein (q_v) is given by:

$$q_v = 2\pi r_v h_v(T_v-T) \qquad (4\text{-}25)$$

where r_a,r_v are the radii of the corresponding artery and vein, h_a, h_v are the convective heat transfer coefficient of the blood vessels calculated as per the steps mentioned in Section 4.2, T_a,T_v is the temperature of the corresponding blood vessel and T is the tissue temperature. Substituting Equations (4-24) and (4-25) in the fifth term of Equation (4-7), we get

$$\int_V [N]\,(q_a+q_v)\,dV = 2\pi r_a h_a \int_0^{\Delta z} \nabla[N](T_a - [N]^T\{T\}^e)dz + 2\pi r_v h_v \int_0^{\Delta z} \nabla[N](T_v - [N]^T\{T\}^e)dz \qquad (4\text{-}26)$$

where Δz is the length of the blood vessel along the edge of the tissue.

The Equations (4-20a), (4-20b), (4-21a), (4-21b), (4-23a), (4-23b), (4-26) represent the terms in Equation (4-7) for the six node and four node spherical elements. The equivalent terms for the triangular and rectangular elements can be obtained from Smith (1991). Substituting for the terms in Equation (4-7) and integrating the equation for all the element surfaces within the given limits yields 38 linear simultaneous equations and 38 unknowns which are the tissue nodal temperatures. Here 38 represent the number of tissue nodes required to build the finger model.

4.1.2.3 Transient Temperature Distribution in Blood Vessels

Galerkin Method is applied in the same way as discussed in the previous section to Equation (3-3).

The above equation is solved with an assumption that the conductive heat transfer in the blood vessels is negligible when compared to the convective heat transfer (Smith 1991). This results in 51 linear simultaneous equations and 51 unknowns which are the blood vessel nodal temperatures. Detailed solution can be found in Smith's Thesis (1991).

4.2 Convective Heat Transfer Coefficient of Blood Vessels

Convective heat transfer coefficients of the blood vessels (h_a, h_v) are calculated using equations from Fundamentals of Heat and Mass Transfer by Incropera and DeWitt.

The steps to calculate the convective heat transfer coefficient are as mentioned below:

a) Blood Velocity(V) is calculated using the below Equation:

$$V = \frac{\left| r_o^{\,2}(P_1 - P_2) \right|}{8\mu\Delta z} \qquad (4\text{-}27)$$

where Δz is the element length, μ is the blood viscosity (7.29*10^-9in mm Hg-hr), P_1 ,P_2 are the pressures at the inlet and the exit of the blood vessel element

b) Reynolds Number (Re) is then calculated using:

$$Re = \frac{\rho_b V 2 r_o}{\mu} \qquad (4\text{-}28)$$

c) If the Reynolds number is less than or equal to 2300, the flow is assumed to be laminar. The flow is turbulent if the Reynolds number is greater than 2300.

d) If the flow is laminar, $h = \frac{4.36k}{2r_o}$ where k is the thermal conductivity of blood(18 in J/hr-cm-C)

e) If the flow is turbulent, $h = \frac{0.023\,\mathrm{Re}^{0.8}\,\mathrm{Pr}^{1/3}\,k}{2r_o}$ where Pr is Prandtl number and is calculated by $\mathrm{Pr} = \frac{\mu C_{p,b}}{k}$.

Here h represents the convective heat transfer coefficient for a given blood vessel. h is h_a for arteries and is h_v for veins.

4.3 Convective Heat Transfer Coefficient of Finger in Different Environments

Convective Heat Transfer coefficient of the finger model in different environmental conditions is calculated by correlating the finger model to a circular cylinder and using the Nusselt number correlation given for the circular cylinder from Fundamentals of Heat and Mass Transfer by Incropera and DeWitt.

The steps to calculate the convective heat transfer coefficient of the finger model is given below:

a) Calculate the thermal conductivity (k), Prandtl number (Pr), kinematic viscosity (υ) of air at the given ambient temperature.

b) Calculate the Reynolds number (Re) using the given airspeed(V_{air}):

$$Re = \frac{V_{air}\,2r_o}{\upsilon} \qquad (4\text{-}29)$$

c) Use the empirical correlation for Nusselt number, to calculate the convective heat transfer coefficient for the finger model(h_c in $\frac{W}{m^2K}$):

$$h_c = \frac{C*\mathrm{Re}^{m}*\mathrm{Pr}^{1/3}*k}{2r_0} \qquad (4\text{-}30)$$

d) The constants C and m in Equation (4-30) are determined by the value of Reynolds number. A table containing the values of C and m for different ranges of Reynolds number is given in Fundamentals of Heat and Mass Transfer by Incropera and DeWitt.

e) The Resistance (R_f) of the finger model in different environmental conditions is :

$$R_f = \frac{1}{h_c} \qquad (4\text{-}31)$$

f) The equivalent resistance of the finger model (R) when a glove of resistance (R_{glove} in $\frac{m^2K}{W}$) is used as protection for the finger is the summation of the resistance of the finger model without glove (R_f) and the resistance of the glove because the resistances are in series.

$$R = R_{glove} + R_f \qquad (4\text{-}32)$$

4.4 Overall Solution Scheme

In the preceding Sections 4.1, 4.2 and 4.3 we have determined the shape functions for each element shape, the pressure distribution, temperature distribution in the tissues and blood vessel, convective heat transfer coefficient of blood vessels. Initial conditions, boundary conditions and thermophysical properties of the tissue and blood have to be assigned before we compute the solution for the finger model. Initial conditions include the initial temperature distribution in tissue and blood vessels, body core temperature and skin temperature. Boundary conditions include the ambient air temperature (T_{air}), convective and radiative heat transfer coefficients (h_c and h_r), relative humidity ($R.H$) and metabolic rate in the finger (generally 1 MET or 21 J/hr-cm^2). The blood nodal pressures and temperatures at the junction where the finger is connected to the hand are also required as a set of boundary conditions. For our study,

George Fu (1995) model has been used to determine these blood pressures and temperatures. The length of the hand in Fu model has been changed accordingly. The body core temperatures and skin temperatures are also determined from Fu (1995) model.

The procedure mentioned in Section 4.1 was followed to obtain a system of equations for the temperature distribution in tissues and blood vessels using the above mentioned set of conditions. These system of equations are numerically solved using the central difference method for a given time step. Using the initial temperature distribution, temperatures for the first time step are obtained by solving the equations using central difference method. Similarly, the temperatures obtained are used to compute the temperatures for the next time step. The same procedure is followed until the temperatures of the last time step are obtained.

In the present study, the human finger model was implemented in MATLAB, and all the required set of conditions are either read from a file or hard coded in the program. The MATLAB program can be modified to obtain different outputs i.e. blood pressures, blood vessel radii, tissue temperatures etc.

The following steps determine how the solution for the Finger Model is obtained:

a) The total length of simulation and time step is determined.

b) The initial and boundary conditions for the finger model are specified. Body skin temperature (Tskin) is modified to include the finger skin temperature (Tsk).

    Tskin = ((18000-(10*Ast))*Tskinb+10*Ast*(Tsk-273.15))/ (18000);

    Where 18000 represents the body surface area in cm^2, Ast is the surface area of the finger, 10 represents the number of fingers.

c) With the core and the new skin temperature, the skin blood vessel radii are obtained using the thermoregulatory Equations (3-8) to (3-12). The sweat rate in g/hr is also computed using the core and skin temperatures.

d) The pressure distribution in the circulatory system of the finger model is obtained with the help of the boundary conditions obtained from Fu (1995) Model.

e) Convective heat transfer coefficient of the blood vessels is calculated following the procedure mentioned in Section 4.2.

f) The temperature distribution in the blood vessels and the tissue is computed.

g) Necessary information like the tissue and blood vessel temperatures, blood vessel pressure distribution is displayed.

h) The variable used to compute the total time of simulation is incremented by the time step used.

i) Steps from b-h are repeated as long as the total time of simulation is not completed. Once the end of simulation is reached, the computer program ends with the required output displayed on the screen.

Chapter 5 - Finger Model Simulation

A three dimensional transient finger thermal model has been developed and solution methods proposed in the earlier chapters. In this chapter, the model will be validated by comparing it against the experimental data. In Section 5.1, the procedure used in the experiments and those used for the model validations will be described and in Section 5.2, the comparisons between the model predictions and experimental results will be presented.

5.1 Experiments

The present 3D finger model will be validated against the experimental results of Wilson et al. (1970) and Santee (1990). Key parameters in the finger model, such as core temperature and skin temperature, require whole body thermal response information. The clothed human model of Fu (1995) will be used to simulate the experiments to obtain necessary input information. Also, the radiant temperature of the environment used will be same as the environment temperature as Wilson (1970) and Santee (1990) used closed chambers to conduct their experiments.

5.1.1 Wilson experiment

Wilson (1970) used a Plexiglas tube to conduct experiments on the human finger. More details about the experimental set up can be found in Section 2.2.2. To validate the current model against Wilson experimental results, the same set of conditions as used by Wilson during his experiments were used for the present simulation. Fu (1995) Model was simulated for 2 hours (first hour for preconditioning) at 25.5^{o}C and 20% RH to obtain input conditions for the 3D finger model. The clothing used on FU Model was Short-sleeve Shirt and Shorts (0.36 clo) to replicate the lightly clothed volunteers involved in Wilson experiments. The current finger model

was preconditioned for one hour at the same experimental conditions using the input data obtained from Fu human model simulation. After the preconditioning, the present 3D model was simulated at a temperature of -15^{o}C in wind speeds of 6.8 m/s, 9m/s and 10m/s with 20% RH for 15 minutes. The finger temperatures were recorded throughout the experiment. The preconditioning stages are important if one hopes to obtain an accurate transient response curve

5.1.2 Santee Experiment

Santee conducted experiments on five volunteers wearing standard cold weather military uniform with three different gloves. Santee's experimental setup has been discussed in detail in Section 2.2.3. To replicate the human body responses as in the original experiment, Fu clothed human Model was simulated for 2 hours at two different temperatures of -6.7 and 0 ^{o}C with Outdoor Ensemble (1.72clo) used as clothing. The finger model was also simulated for the same experimental conditions but with an equivalent convection coefficient (to replicate the effect of gloves). The steps to calculate the equivalent convection coefficient was discussed in Section 4.3. The finger temperatures were recorded during the entire simulation time.

5.2 Model Validation

The three dimensional transient finger model has been developed in the Chapters 3 and 4 and experiments against which the model can be validated have been discussed in the previous section. In the current section, the model predictions and the experimental results are compared.

5.2.1 Validation against Wilson experiment

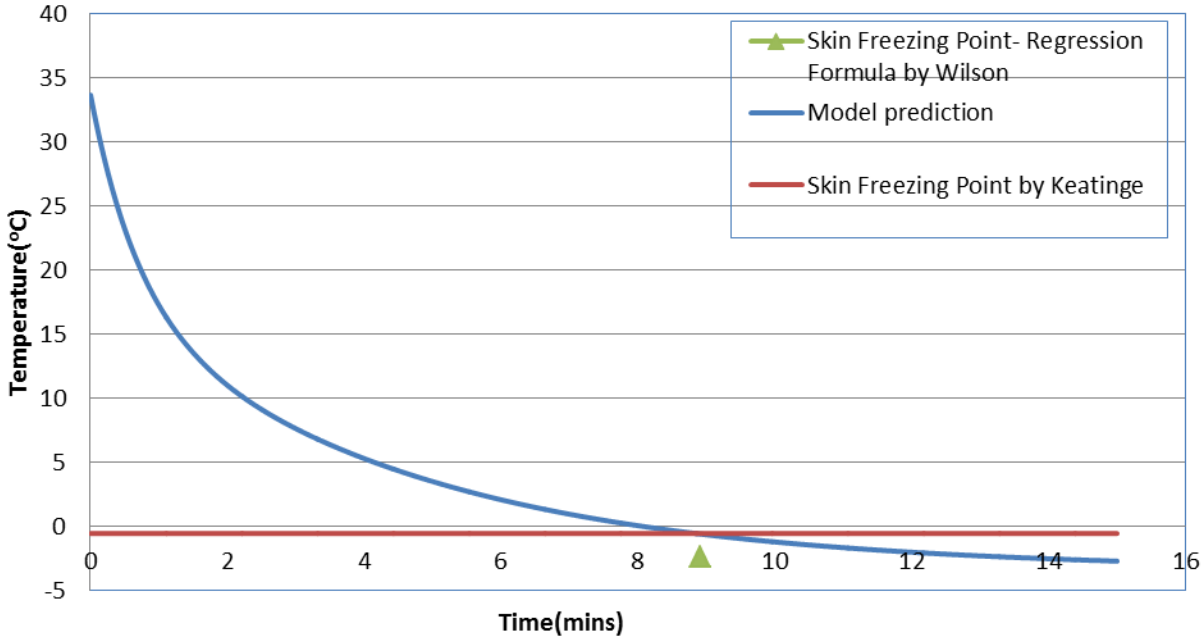

Figure 5.1 Model Prediction for Wilson Experiment in a windspeed of 6.8m/s

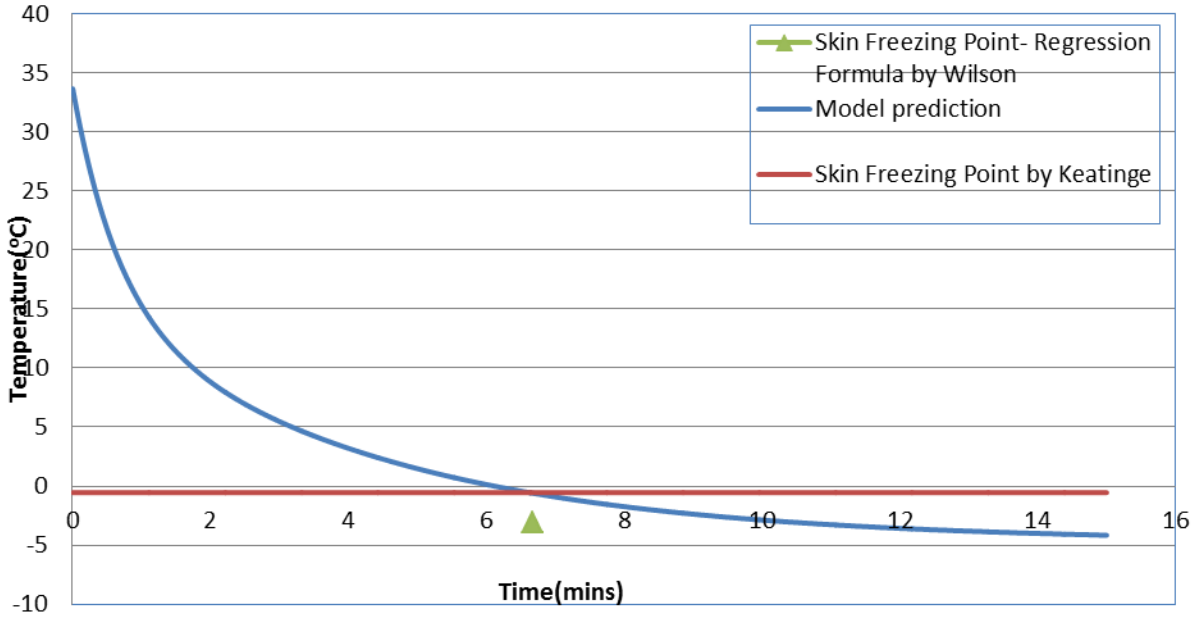

Figure 5.2 Model Prediction for Wilson Experiment in a windspeed of 9m/s

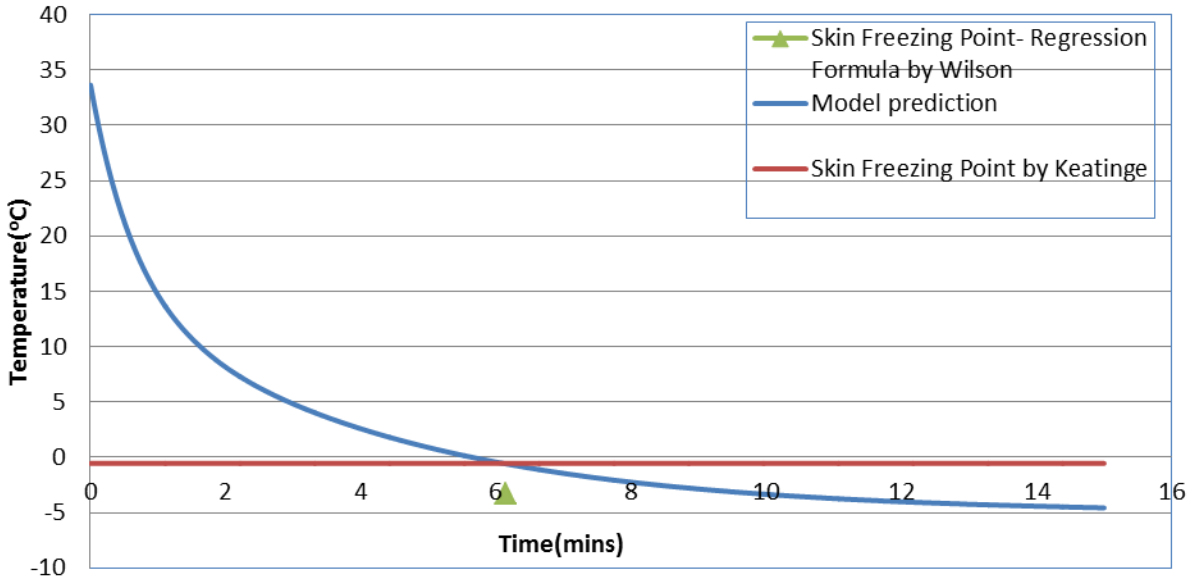

Figure 5.3 Model Prediction for Wilson Experiment in a windspeed of 10m/s

Figures 5.1, 5.2 and 5.3 represent the current model fingertip temperature response to Wilson experimental conditions explained in Section 5.1. The Skin freezing point determined by Keatinge (1960) was between -0.53 and -0.65 ^{o}C and for our experiments, -0.6 ^{o}C was used in the current study as skin freezing point. As shown in Figure 5.1, the fingertip of the current model achieves the skin freezing point in 8.9 minutes and by the end of simulation time of 15 minutes, the fingertip temperature of the current model achieves a temperature of -2.7 ^{o}C. For windspeeds of 9m/s and 10m/s, the finger tip of the current model achieves the skin freezing point in 6.7 and 6.2 minutes. Table 5.1 compares the freezing times calculated by Wilson and those obtained in the current model simulations. Wilson calculated the freezing time from the 147 frost nips obtained in his experiments.

Table 5.1 Comparison of Time to Freeze (minutes) for different windspeeds

Airspeed (m/s)	Time to Freeze(minutes)	
	Wilson Experiment	Current Model
6.8m/s	8.4 ± 2.8	8.9
9m/s	7.1 ± 3.2	6.7
10m/s	6.6 ± 3.1	6.2

From Table 5.1, it can be observed that the freezing times obtained by Wilson and those achieved in the finger model simulations are approximately the same for all the windspeeds. Wilson estimated the apparent freezing point of finger to be -2.4 ± 0.5 ^{o}C for a wind speed of 6.8 m/s, -3.1 ± 0.5 ^{o}C at 9m/s and -3.3 ± 0.4 ^{o}C at 10m/s windspeed. At the end of the current simulation, the fingertip of the model achieved a temperature of -2.7 ^{o}C for a windspeed of 6.8 m/s, -4.1 ^{o}C for a windspeed of 9m/s and -4.6 ^{o}C for a windspeed of 10m/s. From the above analysis, it can be observed that the 3D finger model compares satisfactorily with the experimental results of Wilson et al. (1970).

5.2.2 Validation against Santee experiment

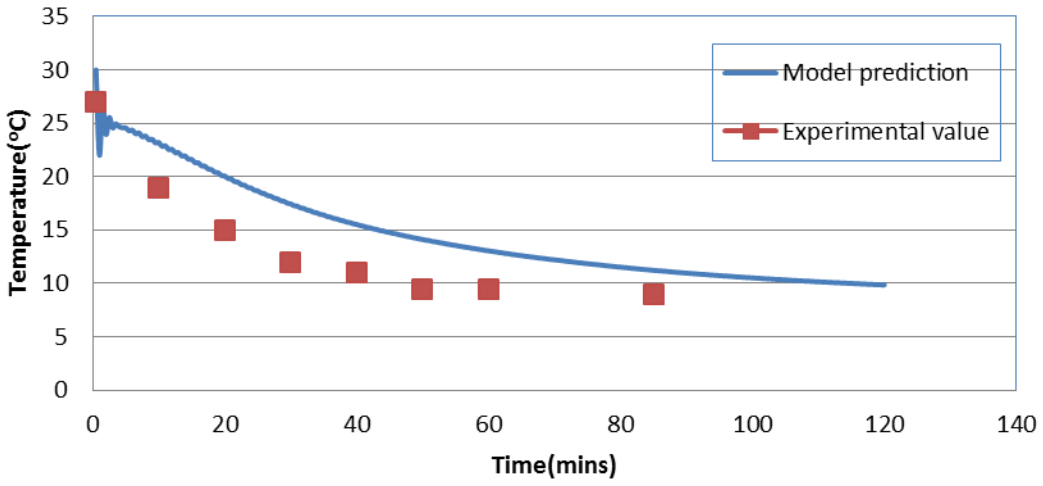

Figure 5.4 Model prediction for Santee Experiment at an ambient temperature of -6.7^{o}C

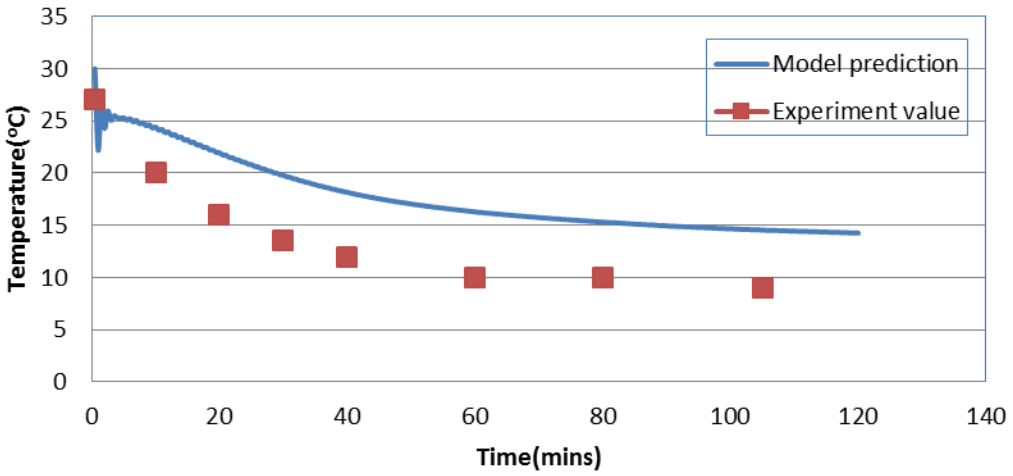

Figure 5.5 Model prediction for Santee Experiment at an ambient temperature of 0°C

Figure 5.4 and 5.5 represents the present model fingertip response to Santee experiments explained in Section 5.1. Santee achieved fingertip temperatures of ~ 9 °C at the end of his experiments as displayed in Figures 5.4 and 5.5. In the current model, the fingertip temperature was 9.87 °C in the ambient temperature of -6.7 °C as displayed in Figure 5-4 and was 14.25 °C in the ambient temperature of 0 °C (Figure 5-5) at the end of the simulation. The current model predicted the fingertip temperatures with an accuracy of 1 °C for ambient temperatures of -6.7 °C and 5°C for ambient temperatures of 0 °C.

The initial disturbance in the model prediction in the Figures 5-4 and 5-5 is due to the large fluctuations in temperature of the model at the beginning of simulation. These large fluctuations in temperatures occurred because the time step chosen for the simulation was 30 seconds. As the FORTRAN Code of Fu clothed human model used to simulate the human response and also to provide input data to the present model wouldn't run for time steps less than 30 seconds, the initial fluctuations in temperature were compromised upon. However, as the

simulation time increased the temperature fluctuations reduced and became zero from where we got a smooth curve for the model prediction.

It can be observed from the above comparisons with Wilson and Santee experiments that the model predictions are consistent with the experimental results for subzero temperatures. However, there is marked difference in temperature when the finger model was compared with the Santee experiment at 0 ^{o}C. One of the reasons for this discrepancy might be the fact that the data obtained from Santee experiment for comparison was of a little finger of a subject whereas the dimension of the current model is higher than that of the little finger. That particular case was selected from Santee experiments because the subject exhibited minimal CIVD response. This was done because the current model doesn't incorporate CIVD. Since the finger model was compared in diverse environmental conditions, it can be concluded that the three dimensional finger model developed in this thesis correctly simulates the transient finger thermal responses of a human being at different temperatures.

Chapter 6 - Results and Discussion

A three dimensional finger model has been developed in Chapters 3 and 4. The three dimensional model was validated against experimental data in Chapter 5. In this chapter, the 3D model will be used to assess the risk of frostbite in humans at different environmental conditions. The current model will also be used to provide information about the gloves to be worn in different environmental conditions in order to prevent frostbite.

To achieve the aforementioned objective, the current model was used to estimate finger temperature with environmental temperatures of 0, -10, -20, -25 and -30 ^{o}C in a windspeed of 0, 3 and 6.8 m/s with three different clothing on the finger. The input conditions for these experiments were obtained from the Fu Body Model simulation which was also run over the same environmental conditions as mentioned above. It is important to note that the clothing used on Fu Model was an outdoor ensemble with a 1.72clo. The finger temperatures were recorded for the entire simulation time.

6.1 Risk of Frostbite

Forty Five simulations have been done with the finger model in different environmental conditions to assess the risk of frostbite. The current model reached the skin freezing point temperature (-0.6^{o}C) in 23 of the experiments. Table 6.1 represents the amount of time taken by the current finger model to reach the skin freezing point temperature (Endurance Time) in these 23 experiments (colored cells). Table 6.2 lists the final fingertip temperature of the current model if frostbite temperature is not achieved in the experiment. All the frostbite cases were also shown in Table 6.2 with different color coding depending on whether the person would survive the entire simulation time without succumbing to hypothermia.

Table 6.1 Endurance Times in minutes at different environmental conditions

clothing		bare	0.4clo	0.8clo
0C	stillair	No	No	No
	3m/s air	No	No	No
	6.8 m/s	No	No	No
-10	stillair	No	No	No
	3m/s air	28	No	No
	6.8 m/s	15.5	No	No
-20	stillair	No	No	No
	3m/s air	13.5	57.5	143
	6.8 m/s	6.5	48	118
-25	stillair	105.5	No	No
	3m/s air	10	44	89
	6.8 m/s	5	37.5	88.5
-30	stillair	78.5	131	No
	3m/s air	8	36	63
	6.8 m/s	4	31	62

Table 6.2 Final Fingertip temperatures (^{o}C) at different environmental conditions

clothing		bare	0.4clo	0.8clo
0C	stillair	14.7	17.05	18.74
	3m/s air	4.51	10.37	14.15
	6.8 m/s	5.19	9.46	13.55
-10	stillair	7.56	10.9	13.31
	3m/s air	**Frostbite**	1.5	6.61
	6.8 m/s	**Frostbite**	0.32	5.82
-20	stillair	-0.1	4.24	7.41
	3m/s air	**Frostbite**	**Frostbite**	**Frostbite**
	6.8 m/s	**Frostbite**	**Frostbite**	**Frostbite**
-25	stillair	**Frostbite**	0.68	4.27
	3m/s air	**Frostbite**	**Frostbite**	**Frostbite**
	6.8 m/s	**Frostbite**	**Frostbite**	**Frostbite**
-30	stillair	**Frostbite**	**Frostbite**	0.99
	3m/s air	**Frostbite**	**Frostbite**	**Frostbite**
	6.8 m/s	**Frostbite**	**Frostbite**	**Frostbite**

Frostbite	Person experiences frostbite before he succumbs to hypothermia
Frostbite	Person experiences frostbite and survives the entire simulation time of 3 hours

From Table 6.1 and 6.2, it can be observed that the person has zero probability of frostbite when the ambient temperature is 0 ^{o}C. Other types of cold injuries are possible at higher temperatures such as loss of dexterity but the current study focuses on frostbite. As the ambient temperatures decrease, the possibility of a person suffering from frostbite increases if proper protective hand gear is not worn. It can be noted from the above tables that as the glove resistance increases, frostbite is less likely to occur. Higher air speeds accelerate the heat loss from the finger which increases the possibility of frostbite. Therefore, ambient temperature, air speed and protective clothing on the finger all play a key role in determining whether the person suffers from frost bite or not. It should also be noted that individual finger and person physiology also play a critical role. The current model is considered a bulk model representing bulk body and finger properties and blood flow and thus is not appropriate to predict any one individual's risk of frostbite without further analysis.

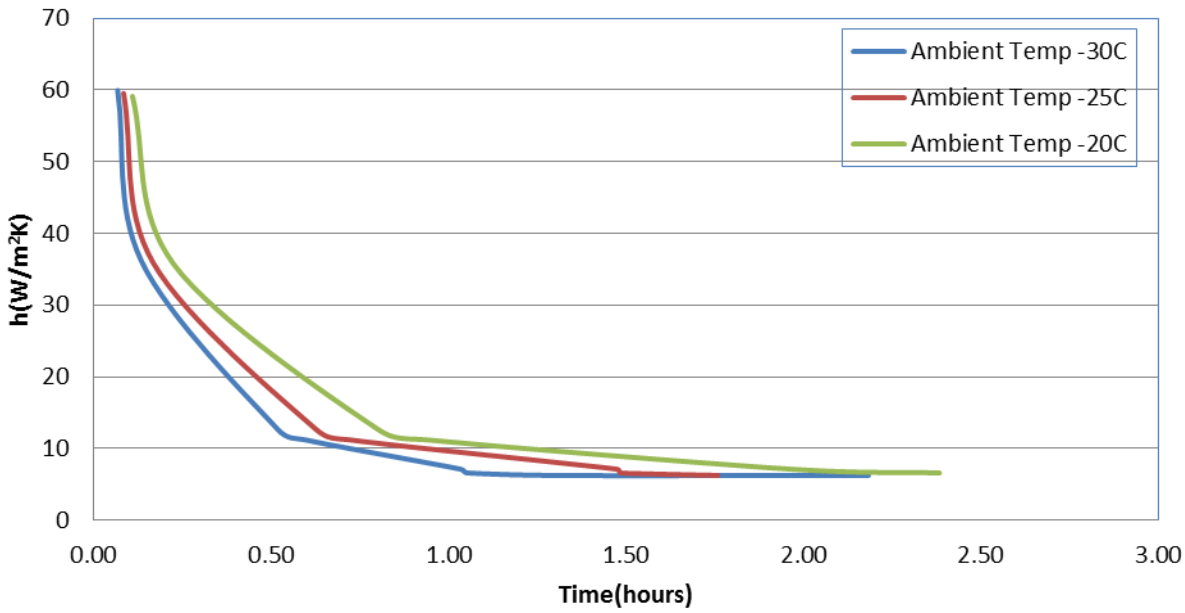

Figure 6.1 Endurance Times for -20, -25 and -30^{o}C Temperatures

Figure 6.1 plots the endurance times of the current model against the heat transfer coefficients used for different environmental conditions. It can be observed from Figure 6.1 that as the heat transfer coefficient increases, the finger tends to freeze faster (endurance times decrease) and vice versa. Ambient temperatures also play a role in accelerating the freezing process as can be seen in the above graph where in an ambient temperature of -30^{o}C, the finger has least endurance times compared to other ambient temperatures.

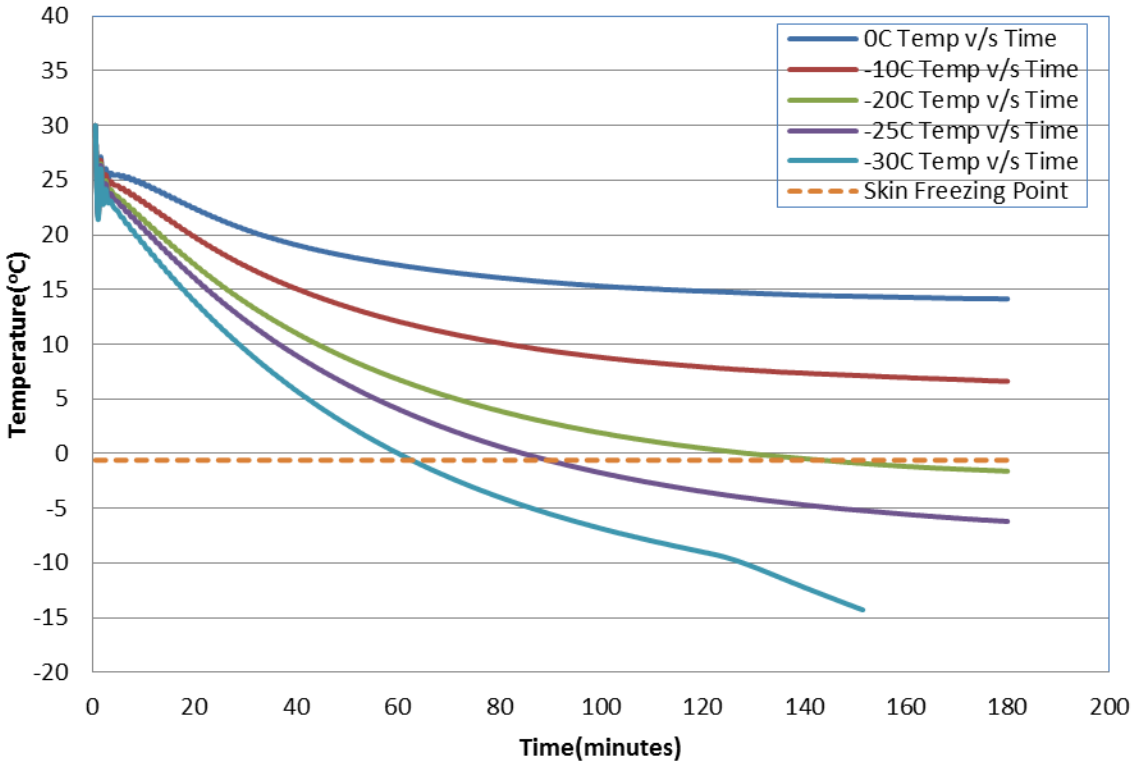

Figure 6.2 Response of a gloved finger (0.8clo) in airspeed of 3m/s at all temperatures

The transient response of a gloved finger (0.8 clo) in ambient temperatures of 0, -10, -20, -25 and -30 ^{o}C at an air speed of 3 m/s has been shown in Figure 6-2. From the graph, it is observed that as the ambient temperature decrease the fingertip temperature decreases more rapidly and the endurance times of finger also reduces. It is evident from Figure 6-2 that the finger has a risk of frostbite when exposed to ambient temperatures of -20, -25 and -30 ^{o}C for the given air speed. The initial disturbance in the temperature is due to the higher time step chosen as discussed in Chapter 5.

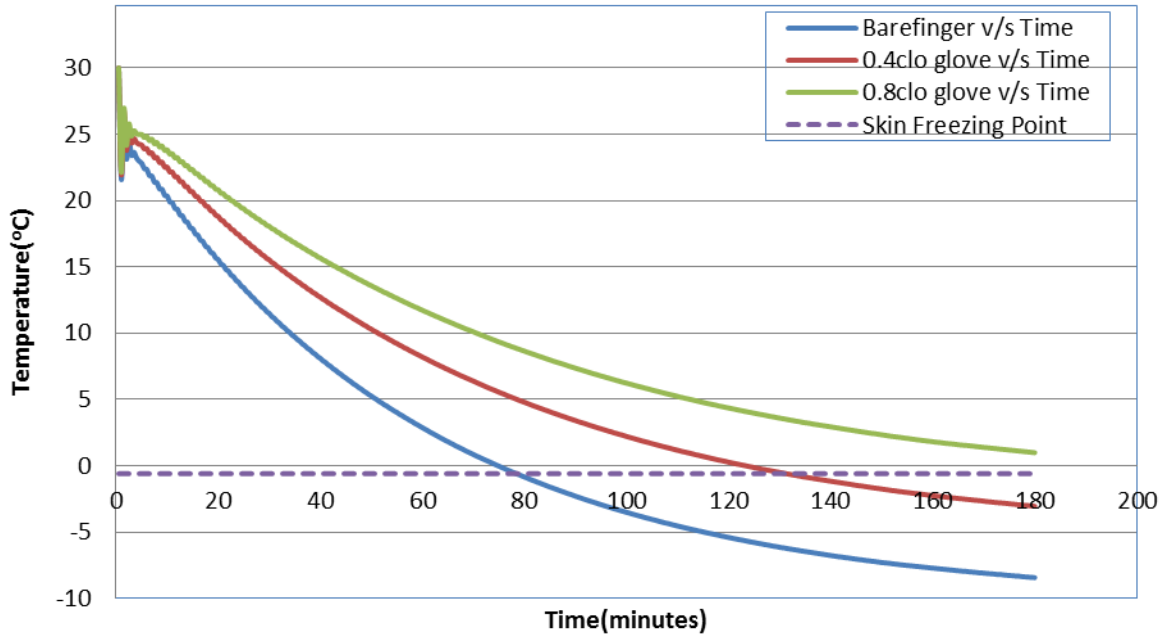

Figure 6.3 Response of finger model wearing different clothing resistances at -30C temperature in still air

Figure 6.3 represents the response of the finger model wearing different glove resistances when exposed to ambient temperature of -30^{o}C in still air. The glove resistances used on the finger model for the simulations were 0, 0.4clo and 0.8 clo. The finger model response from Figure 6.3 indicates that as the glove resistance on the finger reduces, the finger is more susceptible to frostbite. From Figure 6.3, it can be determined that a person wearing 0.8 clo glove will not experience frostbite under the current experimental conditions whereas a person wearing 0.4 clo glove and person without gloves is predicted to experience frostbite.

Frostbite cases in the present finger model experiments have been documented in Table 6.1. These frostbite cases have been plotted on an ambient temperature v/s the total finger resistance graphs. The Y-axis in these graphs represent the ambient temperatures and the X-axis represents the total finger resistance which is the sum of the glove and external convection used in the same experiment. As indicated in Table 6.1, the risk of frostbite is also affected by the exposure times of the finger model to subzero ambient temperatures. Hence, the ambient

temperature v/s total finger resistance graph has been plotted for three different simulation periods – 1hour, 2hour and 3hours.

Figures 6.4, 6.5 and 6.6 show only the frostbite cases in the model experiments. The black square dots plotted in these graphs represent the frostbite cases in the finger model for the given total resistances and ambient temperatures. The green diamond shaped dots represent the threshold total finger resistances which are just enough to prevent any freezing of the finger skin at the given ambient temperatures within the given simulation time.

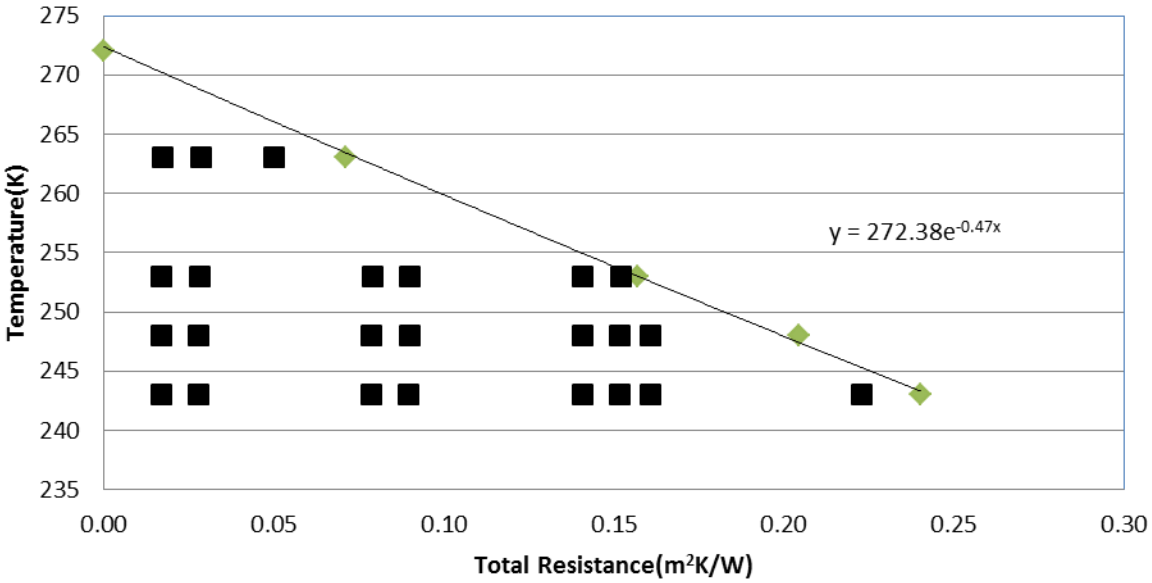

Figure 6.4 Total Resistance of Gloved Finger v/s Ambient Temperature for simulation time of 3 hours

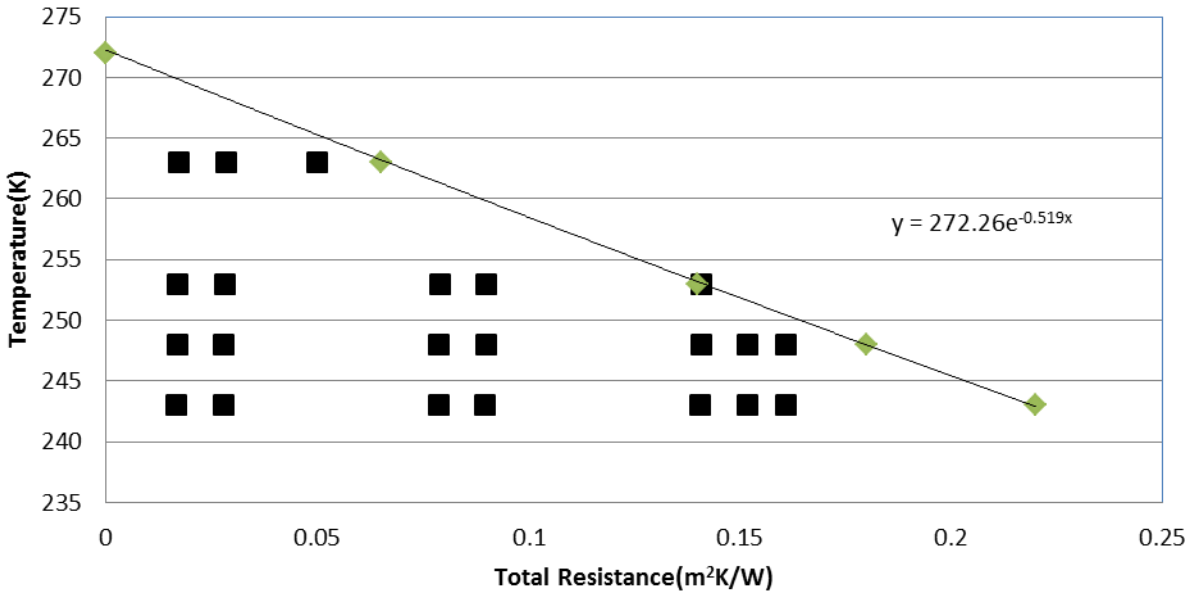

Figure 6.5 Total Resistance of Gloved Finger v/s Ambient Temperature for simulation time of 2 hours

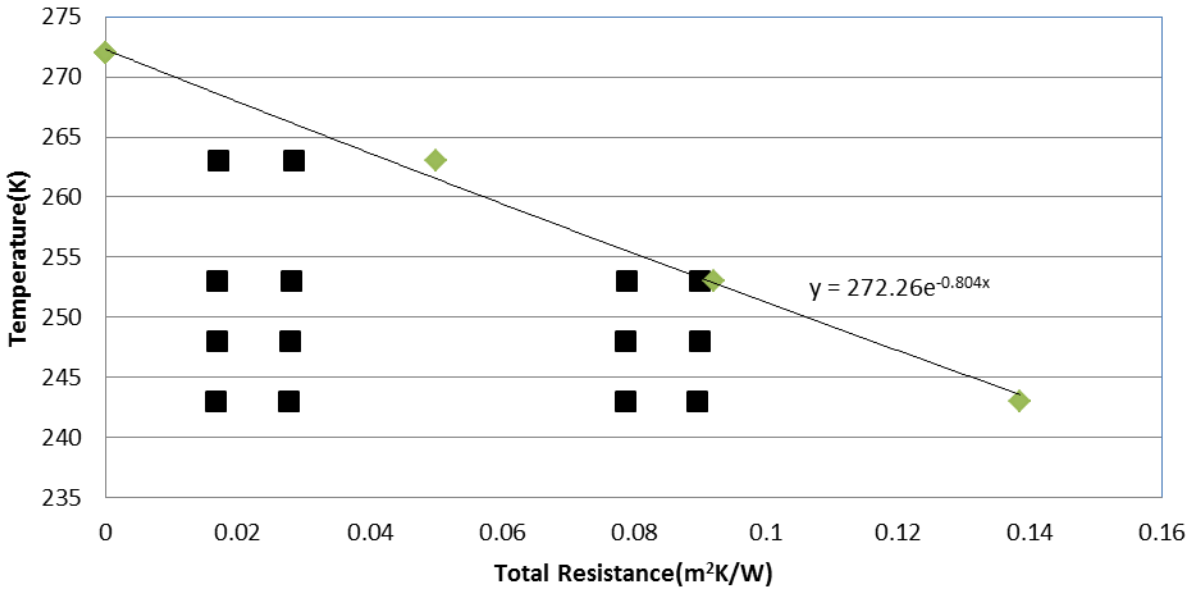

Figure 6.6 Total Resistance of Gloved Finger v/s Ambient Temperature for simulation time of 1 hour

It will be of great interest to know the ambient temperature to which a human finger can be exposed to without any risk of frostbite provided the total finger resistance is known and also to know the resistance of the glove to be worn for any environmental conditions. Hence, using the data from Figures 6-4, 6-5 and 6-6, expressions for the safe ambient temperature (T_{safe}) and safe glove resistance (R_{safe}) has been deduced. The same will be discussed in detail in Section 6.2 and 6.3.

6.2 Expression for safe Ambient Temperature (T_{safe})

Using the safe total resistance values for each simulation period, trend lines of exponential form have been added to all the Figures 6-4, 6-5 and 6-6 which passes through most of the threshold resistance values. As a finger exposed to different temperatures forms a semi-lumped capacitance thermal system thus it is expected that the temperature varies exponentially, exponential trendlines have been chosen.

Using the equation of the trendlines from the above graphs, the general form of the expression for safe ambient temperature is expected to be:

$$T_{safe} = Ke^{CRt} \qquad (6\text{-}1)$$

where, K and C are constants, t is the simulation time in hours and R is the total finger resistance in $\frac{m^2K}{W}$. At this point the resistance is the sum of the clothing and convective resistance on the outside of the finger.

From the equations of the trendlines added to the above graphs, it is evident that the value of constant K is closer to the skin freezing point temperature which is 272.4K or -0.6^{o}C. The other constant C in the equation was derived by minimizing the error in a Least squares method.

The final expression for safe ambient temperature is

$$T_{safe} = (\mathrm{SkFP})e^{-0.775724 Rt^{-0.49111}} \quad (6\text{-}2)$$

Using Equation (6-2), safe ambient temperatures have been calculated for different total finger resistances in different simulation times.

Table 6.3 Safe ambient temperatures (in Kelvin) for different simulation times at different total resistances for the finger

Resistance($\frac{m^2K}{W}$)	3hours	2hours	1hours
0.02	269.95	269.41	268.21
0.04	267.52	266.45	264.08
0.06	265.11	263.53	260.01
0.08	262.72	260.63	256.01
0.1	260.35	257.77	252.07
0.12	258.01	254.94	248.19
0.14	255.69	252.14	244.37
0.16	253.38	249.38	240.60
0.18	251.10	246.64	236.90
0.2	248.84	243.93	233.25
0.22	246.60	241.25	229.66
0.24	244.38	238.61	226.13

To verify the accuracy of the model, the safe temperature values shown in Table 6.3 are compared against the ambient temperatures at the threshold total resistance values obtained from Figures 6.4, 6.5 and 6.6. Figure 6.7 represents the comparison between these two safe ambient temperature values at different simulation times. From Figure 6.7, it can be observed that the expression for T_{safe} calculates the safe ambient temperatures for different total finger resistances and simulation times with reasonable accuracy. From Figure 6.7, it is possible to calculate the safe total finger resistance required when the ambient temperature and exposure time is known or find the safe ambient temperature with no risk of frostbite when the total finger resistance available and exposure time are known.

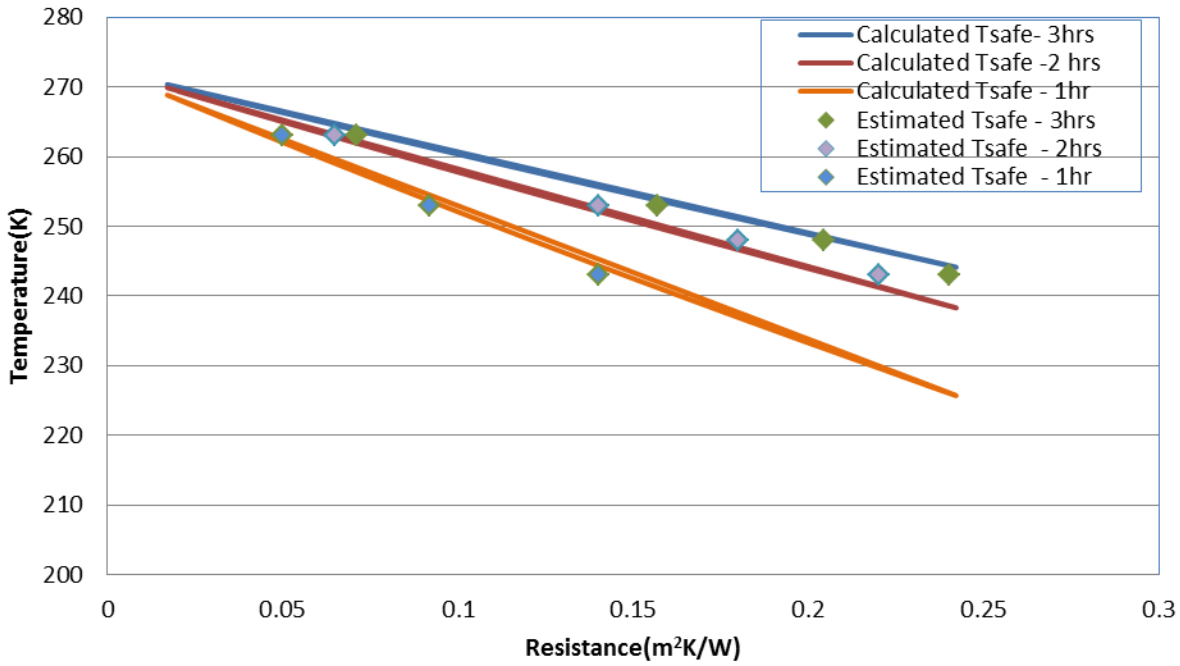

Figure 6.7 Ambient Temperature v/s Total Finger Resistance

6.3 Expression for safe glove resistance (R_{glove})

In Section 6.2, an expression for safe ambient temperature (T_{safe}) was found. Using the same expression, a formula for the safe total finger resistance required at different ambient temperatures and exposure times in order to prevent frost bite can also be found :

$$R_{total} = -\left(\frac{t^{0.4911}}{0.775724}\right) * LN\left(\frac{T}{SkFP}\right) \qquad (6\text{-}3)$$

Using the expression for R_{total}, safe total finger resistances have been calculated for different ambient temperatures and different simulation times. The values of R_{total} (in clo) have been listed in Table 6.4.

Table 6.4 Safe total finger resistances (R_{total} in clo) for different simulation times in different ambient temperatures

Temperature(K)	R_{total} in clo		
	1hour	2hour	3hour
263	0.292	0.411	0.501
253	0.614	0.864	1.054
248	0.780	1.097	1.339
243	0.950	1.335	1.629

Using Equation (6-3), the resistance of the glove to be worn by a person to prevent frostbite in different environmental conditions can be calculated as shown below:

$$\frac{R_{total}}{A_{total}} = \frac{R_{glove}}{A_{glove}} + \frac{1}{h_c . A_s} \qquad (6\text{-}4)$$

where A_{total} is the total surface area of the finger, A_{glove} is the clothed surface area of the finger and A_s is the nude finger surface area.

In the Equation (6-4), $A_{total} = A_{glove}$ and assuming $f_{cl} = 1$ (f_{cl} is a correction factor which is the ratio between the surface area of a clothed body and the nude body surface area, $f_{cl} = A_{glove}/A_s$) With the above assumption, Equation (6-4) reduces to the below format:

$R_{total} = R_{glove} + R_{air}$

$$R_{glove} = R_{total} - R_{air} = -\left(\frac{t^{0.4911}}{0.775724}\right) * \ln\left(\frac{T}{272.4}\right) - \frac{1}{h_c} \qquad (6\text{-}5)$$

where h_c is the heat transfer coefficient for the given environmental conditions calculated as discussed in Section 4.3. The final form of Equation (6-5) provides a very powerful framework for studying frostbite. Additional human studies are recommended to verify the cutoffs and understand population variations. Additional tables and results are presented to demonstrate the power of proposed approach.

The expression for R_{glove} has been used to calculate the safe glove resistance values for different ambient temperatures in windspeeds of 0, 3 and 6.8 m/s. Tables 6.5, 6.6 and 6.7 represent the safe glove resistance values at different ambient temperatures for the three wind speeds. Figures 6.8, 6.9 and 6.10 have been plotted between the safe glove resistance values and the ambient temperatures. From Figure 6.8, 6.9 and 6.10, we can calculate the glove resistance required when the ambient temperature and the exposure time is known in order to prevent frostbite or find the safe ambient temperature when the gloves available and exposure time is known for the three wind speeds.

6.3.1 Air Speed 0 m/s

Using expression 6-5, the glove resistance required at different temperatures and different exposure times in still air have been shown in Table 6-5,

Table 6.5 Glove resistance (clo) required for different ambient temperatures at different simulation times in still air

Temperature(K)	**R_{glove} in clo**		
	1 hour	**2 hour**	**3hour**
263	0	0	0
253	0	0	0.019
248	0	0.058	0.303
243	0	0.297	0.594

The values from Table 6.5 have been plotted in a glove resistance v/s ambient temperature graph in Figure 6.8.

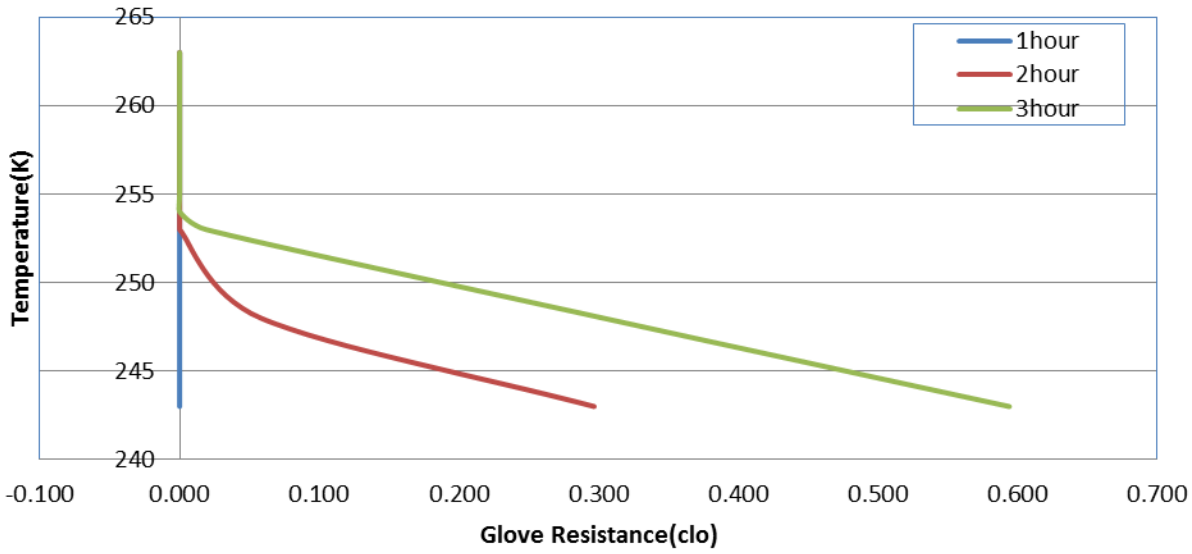

Figure 6.8 Glove Resistance v/s Ambient Temperature at windspeed of 0m/s

It can be observed from Figure 6.8 that a person with no gloves has no risk of frostbite at all ambient temperatures when he/she is exposed for only one hour. However, as the simulation time increases, the amount of glove resistance to be worn by the person to avoid frostbite increases. At an ambient temperature of -30 ^{o}C and exposure time of 3 hours, a person should wear a glove of 0.594 clo resistance to prevent frostbite.

6.3.2 Air Speed 3 m/s

As discussed in Section 6.3.1, Equation (6-5) has been used to calculate the glove resistance at various ambient temperatures and simulation times in airspeed of 3m/s.

Table 6.6 Glove resistance (clo) required for different ambient temperatures at different simulation times in airspeed of 3m/s

Temperature(K)	R_{glove} in clo		
	1 hour	2 hour	3hour
269	0	0	0
268.22	0	0	0.039
266.55	0	0.071	0.129
263	0.11	0.226	0.316
253	0.432	0.684	0.871
248	0.6	0.916	1.161
243	0.774	1.155	1.452

Figure 6.9 plots all the values given in Table 6.6 in a Temperature v/s Glove resistance plot for air speed of 3 m/s. From Figure 6.9, it is possible to match the ambient temperatures and the glove resistance required at that temperature in airspeed of 3 m/s provided that the simulation times are known.

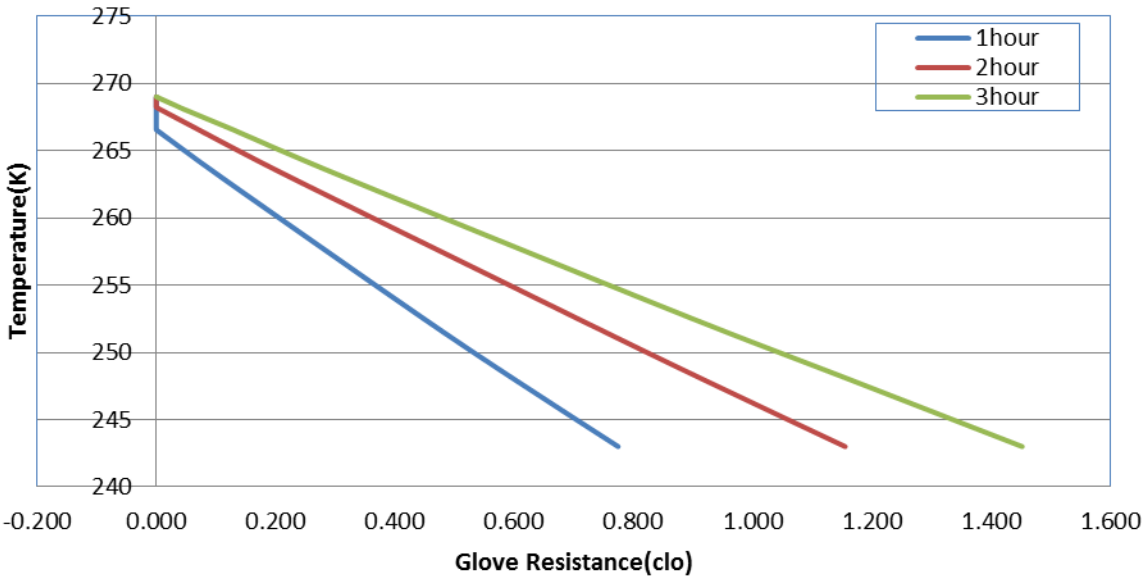

Figure 6.9 Glove Resistance v/s Ambient Temperature at windspeed of 3m/s

6.3.3 Air Speed 6.8 m/s

Table 6.7 represents all the safe glove resistances calculated using Equation (6-5) at different ambient temperatures in airspeed of 6.8 m/s for different simulation times

Table 6.7 Glove resistance (clo) required for different ambient temperatures at different simulation times in airspeed of 6.8 m/s

Temperature(K)	R_{glove} in clo		
	1 hour	2 hour	3hour
270.31	0	0	0
269.86	0	0	0.026
268.83	0	0.045	0.077
263	0.181	0.303	0.394
253	0.503	0.755	0.942
248	0.671	0.987	1.232
243	0.845	1.226	1.523

All the values shown in Table 6.7 has been plotted in Figure 6.10 in a Temperature v/s Resistance plot for air speed of 6.8 m/s.

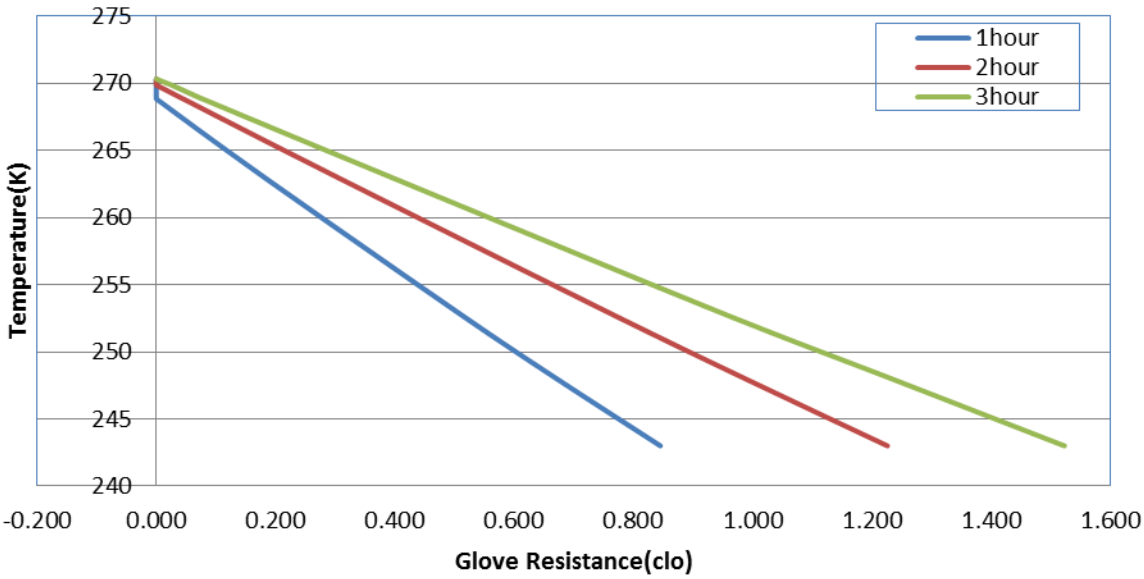

Figure 6.10 Glove Resistance v/s Ambient Temperature at windspeed of 6.8m/s

It can be observed from Figures 6.8, 6.9 and 6.10 that as the windspeed increases, higher glove resistances need to be worn by a person to prevent frostbite at all ambient subzero temperatures. For example: At an ambient temperature of -30 C, one should wear a glove of 0.594 clo resistance in still air, a glove of 1.452 clo resistance in an airspeed of 3 m/s and a glove of 1.523 clo resistance in an airspeed of 6.8 m/s. From Figures 6.8, 6.9 and 6.10, we can also find the glove resistance to be worn by a person when the ambient temperature and exposure time are known in order to prevent frostbite or find the safe ambient temperature when the glove resistance and exposure time is given for any of the three wind speeds.

From the previous discussions, it is apparent that the 3D finger model developed in this thesis can be used to predict the risk of frostbite in humans at different subzero temperatures with reasonable accuracy. Also, the Equations derived in this Chapter can be used to find the appropriate gloves for a given environmental condition and vice versa.

Chapter 7 - Conclusions and Recommendations

The new three dimensional transient finger model was able to predict the risk of frostbite in humans at different environmental conditions. The finger model was validated against Wilson (1976) and Santee (1990) experiments. The model showed good agreement with the Wilson experimental data and with the cold test of Santee experiment. There was a difference of 5 ^{o}C when the model simulation was compared against the warm test of Santee experiment. This was due to the difference in dimensions of the finger used in Santee experiments (little finger) and the current model experiments (dimensions of a bulky middle finger).

The comparisons with Wilson and Santee experiments proved that the finger model can accurately predict the human finger responses in different environmental conditions. Information regarding the resistance of glove required to resist frostbite was obtained when the finger model was simulated in different subzero temperatures in different windspeeds with different resistances on the model. The ambient temperatures in which a finger would not be affected by frostbite with known glove resistances were also found with the help of these simulations. However, this data requires validation against human subjects but it could still serve as a framework in the study of frostbite.

In conclusion, this finger model provides vital information related to the gloves required for specified ambient temperatures to avoid frostbite and also the ambient temperatures up to which a person won't be affected by frostbite with a given set of gloves. The vascular system in the finger model can be improved by inclusion of Arterio-venous anastomoses (AVA), only if more accurate information is available. Inclusion of CIVD in the current finger model would be a major improvement, if the pattern of occurrence of CIVD in humans is well documented.

References

ASHRAE 2005. ASHRAE handbook -Fundamentals. Atlanta Georgia: American Society of Heating, Refrigerating and Air-Conditioning Engineers, Inc.

Atkin, A. R., and C. H. Wyndam. 1969. A study of temperature regulation in the human body with the aid of an analogue computer. Pflugers Archives ges. Physiology 307: 104-19.

Benzinger, T.H. 1970. Peripheral cold reception and central warm reception, sensory mechanisms of behavioral and autonomic thermostasis. Physiological and Behavioral Temperature Regulation Chapter 56: 831-55. Illinois: Charles C. Thomas Publishing Company.

Burton, A.C., 1939. The range and variability of the blood flow in the human fingers and the vasomotor regulation of body temperature. *American Journal of Physiology*, 127:437.

Coffman, J.D., 1972.: Total and nutritional blood flow in the finger. Clinical science.42, 243.

Cooke, J.P., Creager, M.A., Osmundson, P.J. and Shepherd, J.T., 1990. Sex Differences in control of cutaneous blood flow, Journal of the American Heart Association, 82:1607-1615.

Daanen, H.A.M, Koedam, J., Cheun, S.S., 2012, Trainability of cold induced vasodilatation in fingers and toes.

Daanen, H.A.M., 2003, Finger cold induced vasodilation: a review.

Fu, G. 1995. A transient, 3-D mathematical thermal model for the clothed human, Ph.D. dissertation. Kansas State University.

Gagge, A.P., J.A. Stolwijk, and Y. Nishi. 1971. An effective temperature scale based on a simple model of human physiological regulatory response. ASHRAE Transactions 77 Part I: 247-262.

Greenfield, A.D.M., Shepherd, J.T, Whelan, R.F., 1951. The proportion of the total hand blood flow passing through the digits.J.Physiol.113, 63.

Hutton, D.V. 2004. Fundamentals of Finite Element Analysis, 1st ed. New York: McGraw-Hill Book Company.

Incropera, F.P. and DeWitt, D.P. 2002.Fundamentals of Heat and Mass Transfer, 5th ed. New York: John Wiley & sons.

Jones, B.W. and Ogawa, Y., 1992, "Transient Interaction between the Human and the Thermal Environment,: ASHRAE Trans., Vol.98, Part1.

Karaki.W, Ghaddar.N, Ghali.K, 2013, Human thermal response with improved AVA modeling of the digits, International Journal of Thermal Sciences, vol. 67, p. 41-52.

Keatinge, W.R., and P.Cannon.Freezing Point of human skin. Lancet 1:11-14, 1960.

Marieb., 1995,Human Anatomy and Physiology.

Reddy, C.M., Reddy , E.K., and Reddy, B.R.B., 2011. Finite element analysis of blood flow and apply of pressure in the human thumb and applications in disease prevention.International Journal of Science and Advanced Technology, Volume 1 No 2.

Salloum,M., Ghaddar,N., Ghali, K.,2007. A new transient bio-heat model of the human body and its integration to clothing models, International Journal of Thermal Science 46(4) 371-384.

Santee W.R., Endrusick T.L. and Pensotti L.S, 1990. Comparison of light duty gloves with natural and synthetic materials under wet and dry conditions. In: *Advances in Industrial Ergonomics and Safety*, edited by B.Das. London:Taylor & Francis, vol. 2, p. 347-354.

Segerlind, L.J. 1984. Applied Finite Element Analysis, 2nd ed. New York: John Wiley & sons.

Shitzer, A. Stroschein, L., Vital, A.P. Gonzalez, R. R. and pandolf, K. B., 1991,Quantification of conservative endurance times in thermally insulated cold-stressed digits. J. Appl. Physiol. 71(6): p.2528-2535.

Shitzer, A. Stroschein, L., Vital, A.P. Gonzalez, R. R. and pandolf, K. B., 1997, Numerical analysis of an extremity in a cold environment including countercurrent arterio-venous heat exchange, trans.ASME,J.biomech. Eng., 119, p.179-186.

Smith, C.E. 1991. A transient three-dimensional model of the human thermal system, Ph.D. dissertation. Kansas State University.

Stolwijk, J.A. 1970. Mathematical model of thermoregulation, physiological and behavioral temperature regulation Chapter 48: 703-721. Illinois: Charles C. Thomas Publishing Company.

Vanggaard, L., Kuklane, K., Holmer, I. and Smolander, J., 2012.Thermal responses to whole-body cooling in air with special reference to arteriovenous anastomoses in fingers .

Wilson, O., R. F. Goldman, and G. W. Molnar. Freezing temperature of finger skin. 1976.J. Appl. Physiol. 41: 551–558.

Wissler, E.H. 1964. A mathematical model of the human thermal system. Bulletin of Mathematical Biophysics 26(2): p.147-166.

Wissler, E.H. 1966. The use of finite difference techniques in simulating the human thermal system. Physiological and Behavioral Temperature Regulation Chapter 27, p.367-388.

Wissler, E.H. 1985. Mathematical simulation of human thermal behavior using whole body models. Heat and Mass Transfer in Medicine and Biology Chapter 13: 325-373. New York: Plenum Press.

Zweifler, J.A., M.D., Cushing, G., B.A., and Conway, J., M.D., PH.D. 1967. ANGIOLOGY-The journal of vascular diseases, Volume 18, Number 10.

Appendix A - Evaporative Heat Loss

1. Calculate vapor pressure on the skin surface (P_{skin}) = R.H. * P_{skin}^{*}. P_{skin}^{*} is the saturation vapor pressure on the skin surface calculated using the formula mentioned in Smith (1991).
2. Calculate the amount of moisture accumulated on the skin surface(m_{skin})

$$\frac{dm_{skin}}{dt} = m_{rsw} + \frac{P_{skin}^{*} - P_{skin}}{R_{e,s} h_{fg}} - \frac{P_{skin} - P_{ea}}{R_{ea} h_{fg}}$$

   m_{rsw} is the sweat rate obtained from the Equation (3-13), P_{ea} is the vapor pressure of air in kPa, R_{ea} is the evaporative resistance between skin and air in m^2kPa/W, $R_{e,s}$ is the evaporative resistance of skin(0.33 m^2kPa/W from Salloum's Model)

3. If m_{skin} is greater than zero, $P_{skin} = P_{skin}^{*}$.
4. If m_{skin} is equal to zero, P_{skin} is calculated using:

$$P_{skin} = \frac{P_{skin} R_{ea} + P_{ea} R_{es} + m_{rsw} h_{fg} R_{ea} R_{es}}{R_{ea} + R_{es}}$$

5. If P_{skin} is greater than P_{skin}^{*}, then $P_{skin} = P_{skin}^{*}$.
6. The maximum value of m_{skin} is set to 35 g/m^2.
7. Evaporative Heat Loss = ($P_{skin} - P_{ea}$)*h_c*LR where LR is the Lewis Ratio.